Diplomarbeit

Designing a Coplanar Waveguide to manipulate the Scattering Length in a Caesium BEC

zur Erlangung des akademischen Grades

Diplom-Ingenieur

im Rahmen des Studiums

Technische Physik

eingereicht von

Alexander Wiener

Matrikelnummer: 01228902

ausgeführt am Atominstitut
der Fakultät für Physik der Technischen Universität Wien

Betreuung
Betreuer: Univ.Prof. Dipl.-Phys. Dr.rer.nat. Thorsten Schumm
Mitwirkung: Univ.-Ass. Dipl.-Phys. Dr. Stephanie Manz

(Unterschrift Verfasser) (Unterschrift Betreuer)

Wien, February 12, 2020

ABSTRACT: This work aims at implementing a proposal to manipulate the s-wave scattering length of caesium atoms with the magnetic component of a microwave field via Fano-Feshbach resonances. This would open the possibility of controlling the attractive or repulsive properties of the atoms in a Bose-Einstein condensate.
To implement the specific polarized field, which is needed to manipulate the scattering length, a coplanar waveguide (CPW) is designed which can produce the appropriate field strength and orientation. This work outlines the process of designing and simulating the waveguide with the appropriate software as well as the testing of its behaviour. Additionally a short outlook on further developments and how the waveguide will be used in the experimental setup will be given.
The general design of the waveguide takes the form similar to an keyhole with the central geometric element of a circle, which should produce a magnetic field rotating in the plane parallel to the chips surface. The effective field should mainly be a product of the near field and be not radiated into the surroundings. Therefor two principle parameters are important to the design, the circular component of the magnetic field as well as the S-parameter for transmission. Testing for the S-parameter is done conventionally with a vector network analyzer while the measurement of the magnetic field requires a custom setup.

ABRISS: Ziel dieser Arbeit ist die Umsetzung eines Vorschlags zur Manipulation der s-Wellen Streulänge von Cäsiumatomen mit der magnetischen Komponente eines Mikrowellenfeldes über Fano-Feshbach-Resonanzen. Dies würde es möglich machen, die anziehenden oder abstoßenden Eigenschaften der Atome in einem Bose-Einstein-Kondensat zu kontrollieren.
Zur Umsetzung des spezifisch polarisierten Feldes, das zur Manipulation der Streulänge benötigt wird, wird ein koplanarer Wellenleiter (CPW) entworfen, der die entsprechende Feldstärke und Orientierung produzieren kann. Diese Arbeit beschreibt den Prozess des Designs und der Simulation des Wellenleiters mit der entsprechenden Software sowie die experimentelle Prüfung seines Verhaltens. Zusätzlich wird ein kurzer Ausblick auf weitere Entwicklungen und die Verwendung des Wellenleiters im Versuchsaufbau gegeben.
Das allgemeine Design des Wellenleiters nimmt die Form eines Schlüssellochs mit dem zentralen geometrischen Element eines Kreises an, der ein Magnetfeld erzeugen soll, das in der Ebene parallel zur Chip-Oberfläche rotiert. Das effektive Feld sollte hauptsächlich ein Produkt des Nahfeldes sein und nicht in die Umgebung abgestrahlt werden.
Dafür gibt es zwei wesentliche Parameter, die für die Konstruktion wichtig sind, die zirkuläre Komponente des Magnetfeldes sowie den S-Parameter für die Transmission. Die Messung des S-Parameters erfolgt konventionell mit einem vektoriellen Netzwerkanalysator, während die Messung des Magnetfeldes einen eigenen Testaufbau erfordert.

Contents

Chapter 1

The Experiment

The ultimate objective of the experiment is to build a high precision tiltmeter. For that a Bose-Einstein condensate (BEC) of caesium atoms is employed. Via matter wave interferometry a high precision measurement can be done which can be used to determine the relative phase of two caesium BECs.

The basic principle of our experiment is that one caesium BEC is continiously split into two BECs which will conserve their relative phase. Since the evolution of a BEC is dependent on its energy

$$\Psi(t) = e^{-iE(t-t_0)/\hbar} \ \Psi(t_0) \tag{1.1}$$

where Ψ is the wave function of the BEC, t_0 the starting time, t the current time, $\hbar$ the reduced Planck constant and E its energy. The difference in relative phase can be used to determine the energy difference. In our case this energy difference would idealy only stem from a difference in gravitational potential energy from a a tilt between the two BECs respective to earth's gravity.

The use of caesium which promises higher precision than other alkali metals [1], comes however with the trade-off of a more difficult preperation of the BEC. The conventional way of magnetically trapping the atoms and laser cooling them with a later stage of evaporatively cooling until the phase space densitiy is so high that all the atoms occupy the same quantum ground state (only possible for bosonic atoms) results in a problem with caesium. Since the scattering properties of caesium generally are such that the two and three-body inelastic scattering are exothermic the atom cloud heats up for higher densities. To avoid this the absolute ground state $|F = 3, m_F = 3\rangle$ is employed. In this state all the inelastic two-body collisions are supressed at sufficiently low temperatures. This state however is a high-field seeker which cannot be trapped magnetically

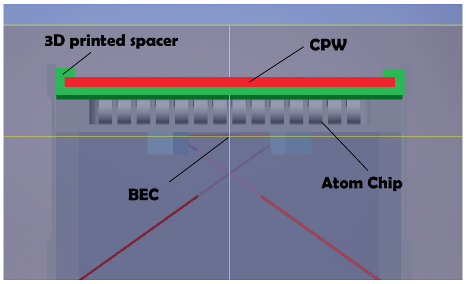

Figure 1.1: A close-up of the top of the UHV cell. At the center of the yellow cross the BEC will be created.

[2]. Additionally to suppressing the two-body inelastic scattering the three-body inelastic scattering needs to be suppressed. This is done via the application of a magnetic field, which is employed to tune the scattering wave length (see 2.3 and 2.4). Since both of these facts don't allow for a magnetic trap, a dipole trap is used instead. For details of this see the diploma thesis of my colleague Max Lerchbaumer [1].

The BEC will be realized in a commercial ColdQuanta system, which includes an atom chip. The whole process of dispensing the caesium atoms, trapping them first in a 2D and later in a 3D magneto-optical trap, cooling them and finally trapping them in the dipole trap naturally has to take place in ultra-high vacuum. The dipole trap is located on an atom chip on the upper side of the vacuum cell. This means that the coplanar waveguide has to be placed outside the vaccum cell on top of the back of the atom chip. For good stability and electrical isolation a 3D printed spacer will be placed between the back of the atom chip and the coplanar waveguide, which results in a distance of approximately 6 mm between the CPW and the BEC. Additionaly the waveguide needs to have a hole for optical access to the BEC.

Chapter 2

Theoretical Discussion

The general objective is to manipulate the scattering length of atoms in a Bose-Einstein condensate via induced microwave radiation. With the microwave radiation one can tune the scattering length (see section 2.3) so that it becomes either negative or positive, which corresponds to attractive or repulsive interaction of the ceasium atoms. Conventionally microwaves are used in creating a caesium BEC in order to pump the atoms from the $F = 3$ ground state to the $F = 4$ state. For this purpose a simple antenna does the trick. In our case however a simple antenna will not suffice because the microwave raditation will need a specific polarisation to affect the caesium atoms in the desired way. A typical helical antenna would not fit into the geometry of the experimental setup due to spatial constraints. To understand how all this can be implemented and tested one needs to have an understanding of several key concepts which will be outlined below.

2.1 Hyperfine Structure in Caesium

The hyperfine splitting in the spectrum of alkali atoms as caesium is caused by the interaction of the electron distribution with the nucleus, specifically their angular momenta. The nuclear magnetic moment

$$\boldsymbol{\mu}_I = \frac{g_I \mu_N}{\hbar} \boldsymbol{I} \tag{2.1}$$

with the nuclear magneton $\mu_N = \frac{e}{2m_p}\hbar$ defined analogous to the Bohr magneton $\mu_B = \frac{e}{2m_e}\hbar$ and the nuclear g-factor g_I. The hyperfine splitting is caused by the interaction of the electron distribution with this nuclear magnetic moment.

Additionally to this effect there are also the quadrupole interaction, the mass effect and the volume shift which lead to considerable differences of frequencies from different isotopes of the same element. [6]. In figure 2.1 the fine and hyperfine structure of caesium for the D2 line is shown.

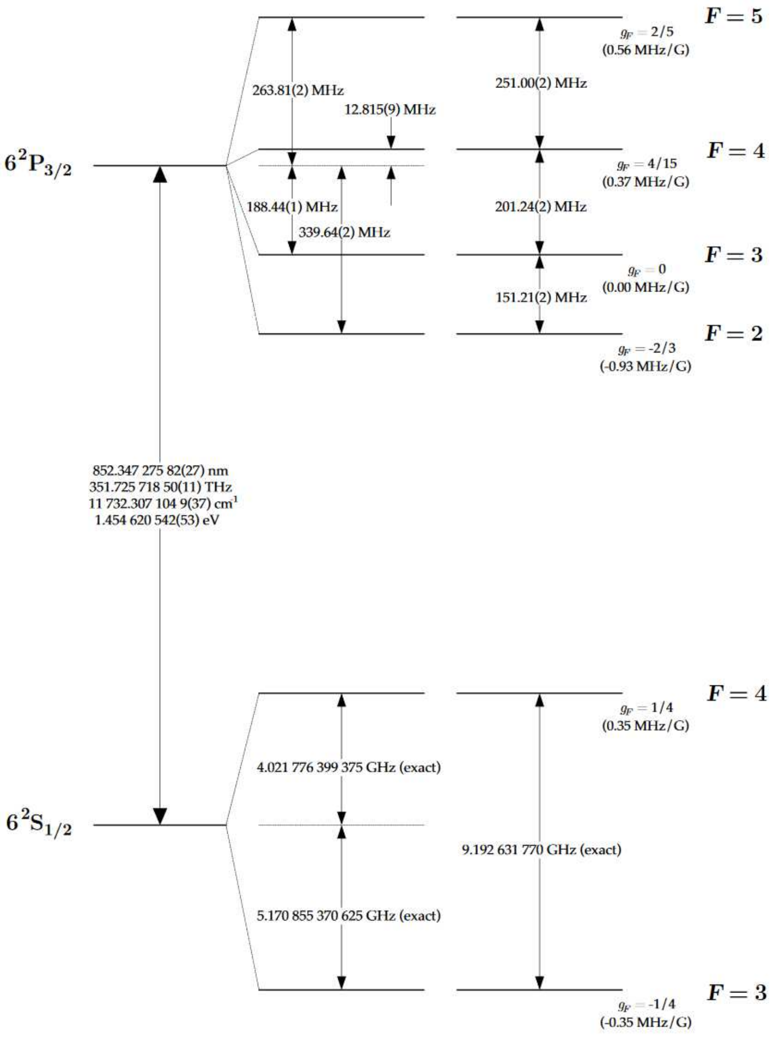

Figure 2.1: The D2 transition hyperfine structure of caesium [4].

2.2 Rabi Frequencies

Rabi frequencies describe the periodic population fluctuation in a two state quantum system. To understand the problem we first have to simplify the system under consideration to a two state system, which can be done for the ground state of the caesium atom which is split by the hyperfine interaction. The resulting states are $F = 3$ and $F = 4$ for the $6^2S_{1/2}$ electronic ground state of ^{133}Cs. The energy of the zero field splitting corresponds to a frequency $f_0 = 2\pi\,\omega_0 \simeq 9.2$ GHz. See figure 2.1. For the calculation of the relevant Rabi frequencies, we follow [5].The microwave field at point $\mathbf{r}$ in the laboratory system is given by

$$\mathbf{B}(\mathbf{r},t) = \frac{1}{2}\big(\hat{\mathbf{B}}(\mathbf{r}))e^{-i\omega t} + \hat{\mathbf{B}}^{*}(\mathbf{r})e^{i\omega t}\big) \tag{2.2}$$

with the microwave frequency ω and the complex phasor

$$\hat{\mathbf{B}}(\mathbf{r}) = \begin{pmatrix} \hat{B_{x'}}(\mathbf{r})e^{-i\phi_x(\mathbf{r})} \\ \hat{B_{y'}}(\mathbf{r})e^{-i\phi_y(\mathbf{r})} \\ \hat{B_{z'}}(\mathbf{r})e^{-i\phi_z(\mathbf{r})} \end{pmatrix} \quad . \tag{2.3}$$

If a homogenous static magnetic field $\mathbf{B}_0$ is applied, a quantisation axis is defined for the atomic states $|F, m_F\rangle$. A new coordinate system is chosen so that the z'-axis is pointing alongside $\mathbf{B}_0$. The coupling of the microwave to the nuclear magnetic moment can be neglected due to the weak coupling [5]. Therefore we only consider the total angular momentum $\mathbf{J}$ (which in the ground state is identical to the spin of the valence electron due to $l = 0$) of the valence electron to the microwave field. The Rabi frequency between the states $|3, m_3\rangle$ and $|4, m_4\rangle$ is given by

$$\Omega^{4,m_4}_{3,m_3} = \frac{2\mu_B}{\hbar}\,\langle 4, m_4|\,\hat{\mathbf{B}}\cdot\mathbf{J}\,|3, m_3\rangle \quad . \tag{2.4}$$

This expression can be reformulated with the ladder operators $J_\pm = J_{x'} \pm iJ_{y'}$ to

$$\begin{aligned} \hat{\mathbf{B}}\cdot\mathbf{J} &= \hat{B_{x'}}e^{-i\phi_x}J_{x'} + \hat{B_{y'}}e^{-i\phi_y}J_{y'} + \hat{B_{z'}}e^{-i\phi_z}J_{z'} \\ &= \frac{1}{2}\big(\hat{B_{x'}}e^{-i\phi_x} - i\hat{B_{y'}}e^{-i\phi_y}\big)J_+ \\ &+ \frac{1}{2}\big(\hat{B_{x'}}e^{-i\phi_x} + i\hat{B_{y'}}e^{-i\phi_y}\big)J_- + \hat{B_{z'}}e^{-i\phi_z}J_{z'} \\ &= \hat{B}_+e^{-i\phi_+}J_+ + \hat{B}_-e^{-i\phi_-}J_- + \hat{B}_\pi e^{-i\phi_\pi} \end{aligned} \tag{2.5}$$

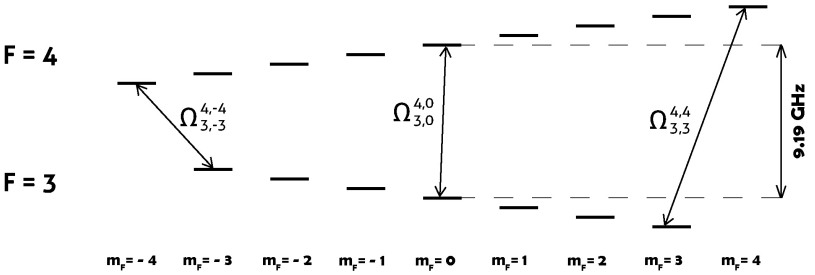

Figure 2.2: The three different non degenerate Rabi frequencies. The different m_F states are split with 0.35 MHz/G and -0.35 MHz/G respectively (Zeeman splitting).

where $\hat{B}_\pi$ and ϕ_π are the real valued amplitude and phase of the component parallel to $\mathbf{B}_0$. $\hat{B}_+$, ϕ_+ and $\hat{B}_-$, ϕ_- the corresponding quantities for the right and left handed circular polarization component.

To characterize the magnetic field component of the microwave field, we are interested in these three transition strengths

$$\begin{aligned}\Omega^{4,-4}_{3,-3} &= \frac{2\mu_B}{\hbar}\langle 4,-4|\,\hat{\mathbf{B}}\cdot\mathbf{J}\,|3,-3\rangle \\ \Omega^{4,0}_{3,0} &= \frac{2\mu_B}{\hbar}\langle 4,0|\,\hat{\mathbf{B}}\cdot\mathbf{J}\,|3,0\rangle \\ \Omega^{4,4}_{3,3} &= \frac{2\mu_B}{\hbar}\langle 4,4|\,\hat{\mathbf{B}}\cdot\mathbf{J}\,|3,3\rangle\end{aligned} \tag{2.6}$$

since they guarantee unique Rabi frequencies. For the first one only the J_--component is nonzero, for the second one only the J_z-component and for the third one the J_+-component is nonzero.

With the results from 2.5 this becomes

$$\begin{aligned}\Omega^{4,-4}_{3,-3} &= \frac{2\mu_B}{\hbar}\hat{B}_-\langle 4,-4|\,J_-\,|3,-3\rangle \\ \Omega^{4,0}_{3,0} &= \frac{2\mu_B}{\hbar}\hat{B}_\pi\langle 4,0|\,J_z\,|3,0\rangle \\ \Omega^{4,4}_{3,3} &= \frac{2\mu_B}{\hbar}\hat{B}_+\langle 4,4|\,J_+\,|3,3\rangle\end{aligned} \tag{2.7}$$

This can be evaluated with the help of the Clebsch-Gordan coefficients (see appendix A) and leads to

$$\begin{aligned} \langle 4,-4| J_- |3,-3\rangle &= -\sqrt{\frac{7}{8}} \\ \langle 4,0| J_z |3,0\rangle &= -\frac{1}{2} \\ \langle 4,4| J_+ |3,3\rangle &= \sqrt{\frac{7}{8}} \end{aligned} \tag{2.8}$$

which in the end results in

$$\begin{aligned} \Omega^{4,-4}_{3,-3} &= -\sqrt{\frac{7}{2}}\frac{\mu_B}{\hbar}\hat{B_-}e^{-i\Phi_-} \\ \Omega^{4,0}_{3,0} &= -\frac{\mu_B}{\hbar}\hat{B_\pi}e^{-i\Phi_z} \\ \Omega^{4,4}_{3,3} &= \sqrt{\frac{7}{2}}\frac{\mu_B}{\hbar}\hat{B_+}e^{-i\Phi_+} \end{aligned} \tag{2.9}$$

With this we can calculate the change in population induced by a short microwave pulse. If for example at time t=0 all the atoms are in state $|4,4\rangle$ and a short microwave pulse of time dt_{MW} follows then the probability of finding the atoms in state $|3,3\rangle$ is [5]

$$p_3 = \frac{n_3}{n_3+n_4} = sin^2(\frac{1}{2}|\Omega^{4,4}_{3,3}|dt_{MW}) \tag{2.10}$$

where n_3 (n_4) is the density of atoms in $|4,4\rangle$ ($|3,3\rangle$).

2.3 Scattering Length

To understand the concept of Fano-Feshbach resonances discussed in the next section, one has to first understand the scattering length. With the scattering length it is possible to describe the effects of any potential apart from its short-range details (i.e. for distances greater than the Van-der-Waals length l_{vdw}). For low energies, as is usually the case for ultracold atoms, only s-wave scattering length matters, which is defined as [2]

$$a = -\lim_{k\to 0}\frac{tan\ \delta_0(k)}{k} \tag{2.11}$$

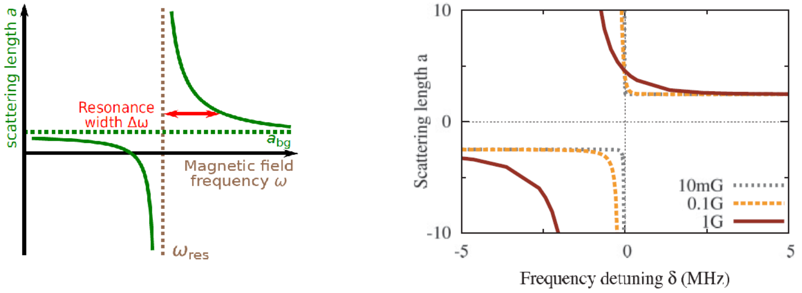

Figure 2.3: (left) The general form of a microwave induced resonance [7]. (right) The scattering length in units of 1000 a_0 as a function of the microwave detuning δ with respect to $\omega_0 \simeq 9.2\ GHz$ [9]. One can see that not only the width increases with higher magnetic fields but also the center of the resonance is shifted.

with the collision wave vector k of the relative motion of the atoms and the phase shift δ_0 between the ingoing and outgoing s-wave.

The scattering length is directly linked to the scattering cross section at low energies. For identical bosons this relation is given by [6]

$$\sigma = 8\pi a^2 \quad , \tag{2.12}$$

which differs from the usual $\sigma = 4\pi a^2$ by a factor of 2. This arises from the fact that the bosons interfere constructively with each other.

The magnitude and sign of the scattering length describe the interaction between atoms. A positive scattering length corresponds to a repulsive interaction. It can be viewed as the radius of a hard sphere from a hard-sphere-potential which can replace the complicated potential for larger scales. A vanishing scattering length corresponds to an effective absence of the mutual interaction (Ramsauer-Townsend effect). Lastly, a negative scattering length is connected to an attractive interaction of the atoms.

The scattering length varies for different internal atomic states, a calculated scattering length for caesium is given in figure 2.5.

With this we have established and quantified the interaction of a magentic field and fluctuations in the population of $F = 3$ and $F = 4$. This will be used later for a procedure to test the magentic field produced by the CPW.

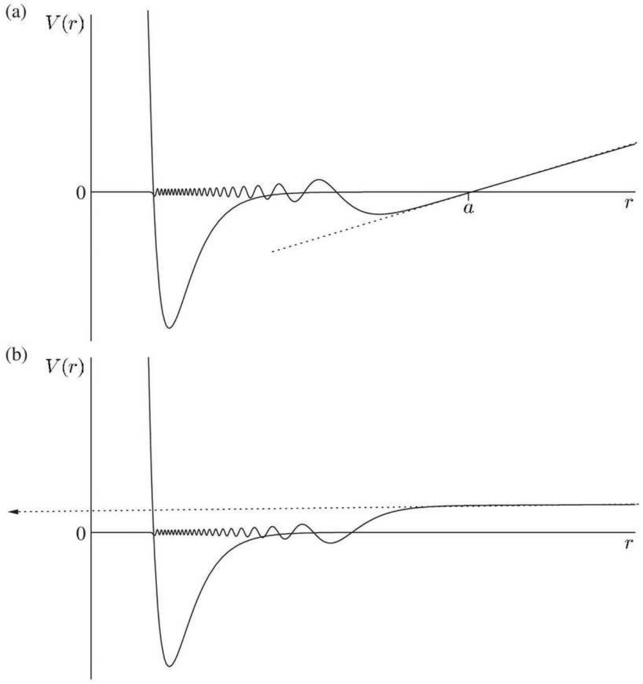

Figure 2.4: The wavefunction $P(r) = rR(r)$ for low energy scattering for different potentials can bring about a positive scattering length (a) or a negative scattering length (b). The scattering length can be found by extrapolating the long range behaviour of the wavefunction and finding the crossing point with the abscissa (dashed line) [6].

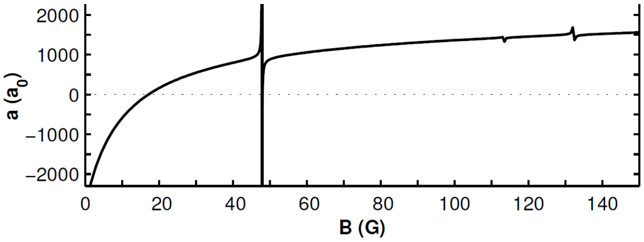

Figure 2.5: Calculated scattering length for absolute ground state ($F = 3$, $m_F = 3$) caesium over the magnetic field strength B in units of the Bohr radius a_0 [2].

2.4 Fano-Feshbach Resonances

The central premise of this work is that one can tune the interactions of ultracold alkali atoms via an applied microwave field. Following [7] we will discuss the theoretical foundations of our experimental approach. The work of Papoular [7] suggests feasible experimental parameters in the case of caesium.

Let us consider the radial symmetric potential for the mutual interaction of two alkali atoms in their ground state (see figure 2.6). For large distances this takes the form of a Van-der-Waals potential. It has an inner repulsive core and for long distance the potential goes to zero. Inbetween is a minimum which may allow bound states.

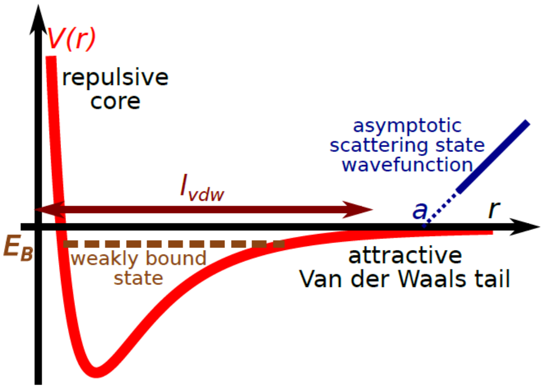

Figure 2.6: The interatomic potential for the interaction of two alkali atoms in their ground state. l_{vdw} is the Van-der-Waals length and a the scattering length [7].

In the next step this rather complicated model is replaced by a simply square well, which is characterized fully by its depth ($|E_D|$) and width (l). The width is chosen to be close to the Van-der-Waals length l_{vdw}. The potential is shown in figure 2.7.

The scattering properties of this potential well are well known [8]. The s-wave scattering length a satisfies the following relation

$$1-\frac{a}{l}=\frac{tan(k_D l)}{k_D l} \quad , \tag{2.13}$$

where $k_D l = \sqrt{|E_D|/E_l}$ and $E_l = \hbar^2/(2m_r l^2)$ (with the reduced mass of the two identical atoms $m_r = \frac{1}{2}m$). The bound state energies are given by $E_B = -E_l(\kappa l)^2$ where κ and k are related via the following two equations

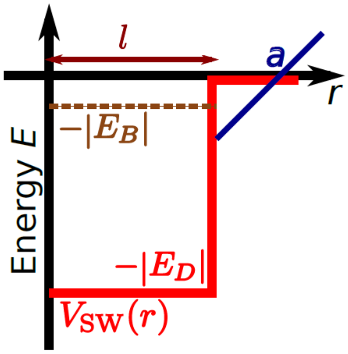

Figure 2.7: The simplified square potential[7].

$$\begin{aligned} (k_D l)^2 &= (\kappa l)^2 + (kl)^2 \\ \kappa l &= -\frac{kl}{tan(kl)} \quad . \end{aligned} \tag{2.14}$$

For a given width l and depth $|E_D|$ the number of bound states n_B is determined by the following inequality

$$(2n_B - 1)\frac{\pi}{2} < k_D l < (2n_B + 1)\frac{\pi}{2} \quad . \tag{2.15}$$

In figure 2.8 the scattering length a and the bound energies E_B are plotted. This shows the relation of the scattering length to the position of the highest bound state energy. When increasing the well depth so that a new bound state becomes possible the scattering length diverges to $-\infty$ until a new bound state is possible. As soon as this happens and the well is able to support a new weakly bound state, it becomes a large positive number. This shows the connection of the scattering length to the existence of weakly bound states.

We will now discuss what happens to an atomic collision in presence of the microwave field. It is tuned close to the hyperfine transition frequency ω_{hf}. If one of the atoms absorbs one microwave photon, the atom pair becomes excited in the two level picture. The ground state $|g\rangle$ and the excited state $|e\rangle$ differ by the energy of the absorbed microwave photon $\Delta E_{hf} = \hbar\omega_{hf}$. These potentials can be simplified to square wells, however it should be noted that a real physical potential with similar characteristics shows the same behaviour. The two different potentials V_g and V_e are shown in figure 2.9.

It is assumed that V_e supports a weakly bound dimer state with binding energy $|E_T|$. When the frequency of the microwave field is close to the energy

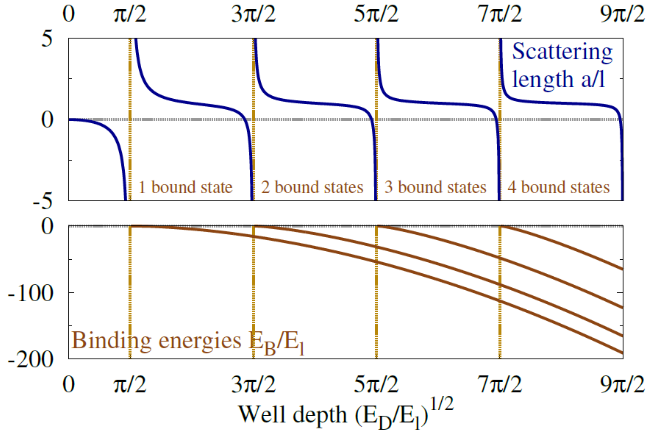

Figure 2.8: The scattering length and the bound state energies [7].

difference $\hbar\omega_{res}^0 = \Delta E_{hf} - |E_T|$ between the threshold energy of the ground potential well and the bound state this bound state can either just exist or is just out of reach. This leads to the behaviour of the scattering length discussed above: When the well depth approaches a magnitude, which can support a weakly bound state, a scattering resonance occurs. The divergence of the scattering length - for frequencies close to the resonant frequencies - can be described by

$$a(\omega) = a_{bg}\left(1 + \frac{\Delta\omega}{\omega - \omega_{res}}\right) \tag{2.16}$$

where a_{bg} is the background scattering length, ω_{res} and $\Delta\omega$ is the resonance width (see figure 2.9).

This resonance width is proportional to the square of the amplitude of the oscillating field B_{osc}^2. Due to the coupling of $|g\rangle$ and $|e\rangle$ by the microwave radiation a slight shift away from ω_{res}^0 occurs

$$\omega_{res} = \omega_{res}^0 + \alpha B_{osc}^2 \tag{2.17}$$

where α is the resonance shift. With the method of the square wells the resonance shift α and the resonance width $\Delta\omega$ can be calculated, a more precise calculation can be done by a so called coupled channel approach [7]. This leads to the following results for a B_{osc} of 1G for caesium: [9]

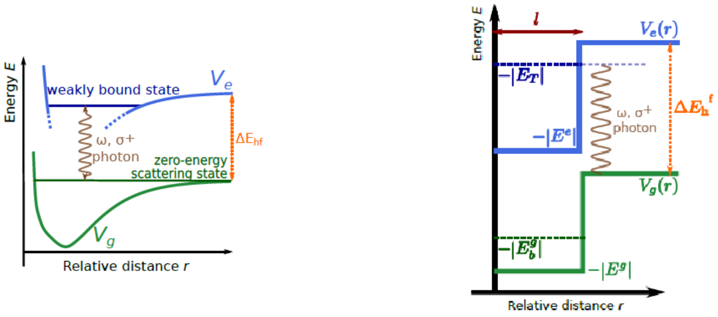

Figure 2.9: The two physical potentials (left) and the two square wells (right) for the ground and excited states $|g\rangle$ and $|e\rangle$ [7].

$$\begin{aligned} \alpha &= 30 \;\; kHz/G^2 \\ \Delta\omega/2\pi &= -4.5 \;\; kHz \end{aligned} \tag{2.18}$$

2.5 Coplanar Waveguides

To produce a microwave field for the Fano-Feshbach resonance mentioned above, we want to employ a Coplanar Waveguide. Coplanar Waveguides were first introduced by Cheng P. Wen [10]. In general they consist of a thin strip of conducting material on a piece of dielectric material. On both sides of the conducting middle strip there are two gaps after which a (generally) wider area of metallization starts (see figure 2.10). Coplanar waveguides as their name suggests are used to convey microwaves (the coplanar part of the name comes from the fact that all 3 metallizations are on the same plane). In our case the purpose of the waveguide is to produce a certain magnetic field configuration at the position of the atoms.

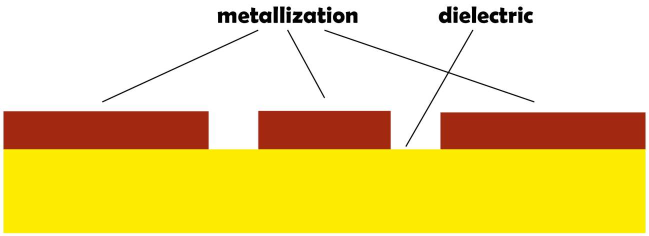

Figure 2.10: Vertical cut through a coplanar waveguide.

2.5.1 Wave Impedance and Characteristic Impedance

Wave impedance and characteristic impedance are important for coplanar waveguides and microwave transmission in general.

Wave impedance is the ratio of the magnetic to the electric transverse component of a given electromagnetic wave [12].

$$Z = \frac{E_0^-(x)}{H_0^-(x)} \tag{2.19}$$

where $E_0^-(x)$ and $H_0^-(x)$ are given in the phasor representation. The ratio of electric and magnetic field has the dimension of a resistance, corresponding to the unit [Ohm] in SI units. The wave impedance is commonly given in Ohm. It is however not a physical resistance as measured by an Ohmmeter. For a lossless, non conducting material (i.e. a perfect dielectric) with a relative permeability $\mu_r = 1$ the wave impedance is given by [12]:

$$\eta = \frac{\eta_0}{\sqrt{\epsilon_r}} = \frac{\sqrt{\epsilon_0/\mu_0}}{\sqrt{\epsilon_r}} \approx \frac{377\ \Omega}{\sqrt{\epsilon_r}} \tag{2.20}$$

where η_0 is the wave impedance of free space, ϵ_0 the vacuum permittivity, μ_0 the vacuum permeability and ϵ_r the relative permittivity of the medium.

The characteristic impedance on the other hand is dependent on the concrete geometry of the transmission line. The characteristic impedance relates the voltage (V_0) and current (I_0) of a travelling wave[12]

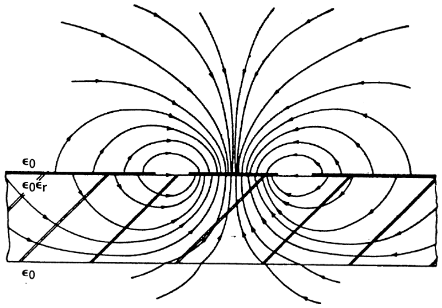

Figure 2.11: The electric field distribution of a coplanar waveguide in a vertical cut through a CPW [11].

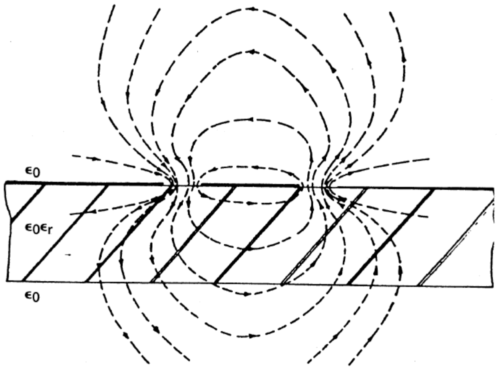

Figure 2.12: The magnetic field distribution of a coplanar waveguide in a vertical cut through a CPW [11].

$$Z_0 = \frac{V_0}{I_0} \quad . \tag{2.21}$$

For an incremental length an equivalent circuit can be given (see figure 2.13).

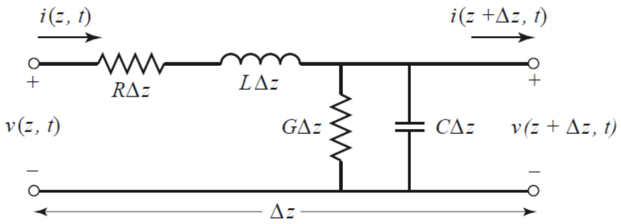

Figure 2.13: Lumped-element eqivalent of an incremental length of the transmission line.[12]

With this one can evaluate 2.21 [12]

$$Z_0 = \sqrt{\frac{R + i\omega L}{G + i\omega C}} \quad , \tag{2.22}$$

which simplifies for a lossless transmission to

$$Z_0 = \sqrt{\frac{L}{C}} \quad , \tag{2.23}$$

where L is the inductance and C the capacitance per unit length. There are a number of analytical methods for different geometries some of them are discussed in [13]. However the easiest and most convenient method of calculating the characteristic impedance of a certain geometry are the online available calculators, for example in the already useful microwave101.com [14] or the more comprehensive [15].

2.5.2 Impedance Matching

The purpose of determining the characteristic impedance of different sections of the coplanar waveguide is important in order to reduce internal signal reflection and to maximize the transfer of power. One can in this context think of the optical analogon of the refractive index of light in a medium. When a beam of light enters from one medium with a specific refractive index into another with a different refractive index then reflections occur. The same is true for the characteristic impedance. One needs to take care that the standard of 50 Ohms of characteristic impedance is kept as consistently as possible to avoid reflections. [12]

The reflection coefficient Γ which is the complex ratio of reflected wave to the incoming wave

$$\Gamma = \frac{V^-}{V^+} \tag{2.24}$$

can be written in terms of the characteristic impedance and the load impedance

$$\Gamma = \frac{Z_L - Z_0}{Z_L + Z_0} \quad . \tag{2.25}$$

One can easily see that Γ becomes 0 when the characteristic impedance matches the load impedance.

2.5.3 Scattering Parameters

The Scattering parameters (or S-parameters) are used to described the transmission and reflection characteristics of a linear N-port system - in our case a two port coplanar waveguide. The S-Parameters are the elements of an N×N dimensional matrix, the Scattering Matrix. This matrix relates the ingoing to the outgoing amplitudes of voltage waves [12].

$$\begin{bmatrix} V_1^- \\ V_2^- \\ \vdots \\ V_N^- \end{bmatrix} = \begin{bmatrix} S_{11} & S_{12} & \dots & S_{1N} \\ S_{21} & S_{22} & \dots & S_{2N} \\ \vdots & \vdots & \ddots & \vdots \\ S_{N1} & S_{N2} & \dots & S_{NN} \end{bmatrix} \begin{bmatrix} V_1^+ \\ V_2^+ \\ \vdots \\ V_N^+ \end{bmatrix} \tag{2.26}$$

where V_i^- and V_i^+ (i from 0 to N) describe the outgoing and ingoing voltage amplitudes. The S-parameters with the same indices are therefore a measure of how much of the incident voltage amplitude gets reflected back out of the same port. The S-parameters with different indices describe how much of the incident voltage amplitude is transmitted from one port to the other.

The S-Parameters can be used as a measure of the qualitity of impedance matching of the characteristic impedances of a network.

2.5.4 Units

In the field of microwave engineering one normally thinks in terms of power and not in terms of current or voltage. Due to the fact that generally a characteristic impedance of 50 Ohm is used this can easily be used to relate the power to current. With the well known formulas

$$\begin{aligned} P &= UI \\ U &= RI \\ P &= \frac{U^2}{R} \\ P &= I^2R \end{aligned} \tag{2.27}$$

and the fact that the characteristic impedance is 50 Ohm,

$$\begin{aligned} P &= \frac{U^2}{50} \\ P &= 50I^2 \end{aligned} \tag{2.28}$$

The normal convention of units in microwave electronics is decibel-milliwatts (dBm) for absolute power and decibel (dB) for relative amplification or attenuation, its logarithmic definitions makes it easy to simply add those up without needing to multiple.

$$P[dBm] = 10\ log_{10}\left(\frac{P[mW]}{1\ mW}\right) \quad . \tag{2.29}$$

A similar relation is used to define decibel for a ratio of two power levels P_1 and P_2. The attenuation or amplification L in decibel is then given as

$$L[dB] = 10\,log_{10}\Big(\frac{P_1[W]}{P_2[W]}\Big) \qquad . \tag{2.30}$$

Chapter 3

Simulation and Design

3.1 The Workflow

Since calculating the microwave behaviour of this specific geometry analytically is not an option one has to rely on numerical simulations. These were done with COMSOL Multiphysics (from here on simply called Comsol), for details see the section below. The software used for preparing the printable circuit board files was Autodesk EAGLE (from here on simply called Eagle) we did not find a simple way to get the simulated geometry from Comsol to Eagle, but had to use the workflow outlined below.

The reason we start with the workflow in Comsol is that we started with simulating our geometry there (see section 3.2). One can easily design the geometry and access all desired parameters at a later point as well. After arriving at a satisfactory geometry, which involves Comsol's primary function of simulating physics, auxilliary polygons are designed. These polygons contain every point which is of importance for later drawing in Inventor. The polygon points are defined as variable-dependant parameters which means that they change easily with an iteration in the parameters resulting from, for example, an improved geometry from a simulation. The points representing these polygons can be accesed as a list, which can be imported easily into a spreadsheet program like Excel.

In Excel one has to convert the coordinates from variable-dependent parameters to fixed numerical values which can easily done by defining the values for this specific geometry and converting the coordinates of the points in formulae which take in the values of the parameters and give the numerical values. Then only the numerical values are saved in a seperate Excel sheet in the XLS (or XLSX) file format.

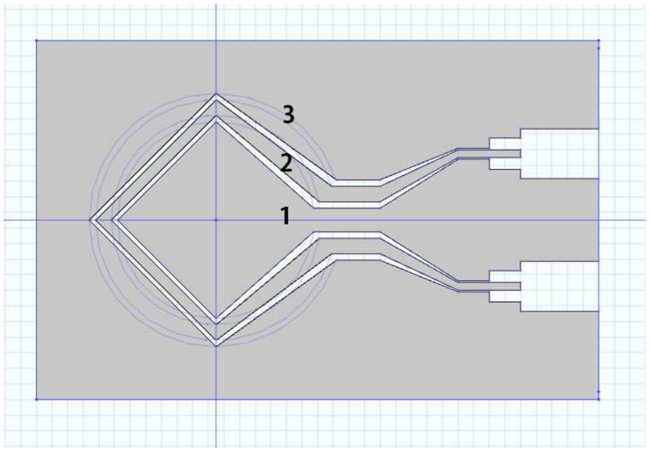

Figure 3.1: The three polygons (numbered) which are used to acurately construct the geometry in Inventor. The inner hole of the final geometry is missing because it is easily constructed with its known dimensions anyway. The auxiliary lines are the outlines of the correct geometry.

When creating a sketch in Inventor one can import points from these XLS or XLSX files. Then one can easily draw the geometry by literally connecting the dots with straight lines and arcs. This process is preferable to just drawing each geometry from scratch because by simply changing the parameters in the Excel sheet one can efficiently change the numerical values of the coordinates of the important point which translates quite quickly into a changed geometry. Then the geometry in Inventor is exported in the DXF file format which is then imported in Eagle. One has, however, to be careful to set the scale and line width to the correct values (which we found by trial and error) so that a useful geometry is imported rather than a cluster of blobs.

It is probably not the most efficient workflow possible, but the most efficient one we could come up with. It takes us from simulating and designing in Comsol via Microsoft Excel to Autodesk Inventor and finally ends in a printable circuit board (PCB) design in Eagle. The reason for this rather tedious path is that to our knowledge there is no easily compatible file format that can be transfered from Comsol into Eagle. It is, however, possible to import geometries from Inventor to EAGLE. In the beginning we had hoped that we could simply find a file format that could import the geometry from Comsol to inventor. We could, however, only find a file format (STL) that could import the Comsol mesh into Inventor, which is unfortunately rather useless for our problem. Similarly it is also not an option to simply redraw the geometry in Inventor because of the way we could (or rather could not) access the geometric parameters of your objects after one has drawn them. In the end we came up with a rather cumbersome workaround which is outlined below.

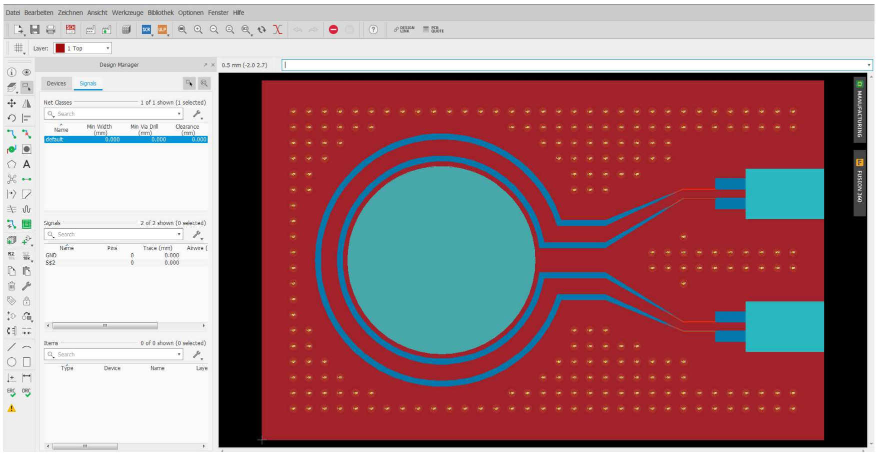

Figure 3.2: A Screenshot from Eagle: The red areas correspond to metallisation, the blue areas are not metallised, the cyan ares are milled out and the dots are vias.

Eagle is a program for designing printable circuit boards. It works with different layers for different applications, for example layer 1 is the top layer of metallisation, layer 16 is the bottom layer of metallisation. With the imported geometry one has to define which areas are part of the top metallisation and which layers need to be cut out (layer 46, milling). Furthermore, one has to draw the total dimension (layer 20) and create vias. A so-called via (latin for path) is a hole coated with electrically conducting material which acts as an electrical connection between different layers of the microwave chip (in our case only top and bottom). All this has to be done in accordance with the design rules of the printing company B. To see the design in the Eagle user interface see figure 3.2.

3.2 Simulation in Comsol Multiphysics

COMSOL Multiphysics is a software to analyse numerical physical problems. It has a *Radio Frequency* (RF) module which is used to simulate antennas, waveguide, filters and more. In our case it was used to simulate the coplanar waveguide. There are essentially two different properties we are interested in when designing our CPW. The first properties are the S-parameters which are discussed in section 2.5 and the second is the electromagnetic near field, specifically its magnetic component.

For the case of a two-port system, the S_{11} describes the proportion of the incident voltage amplitude in Port 1, that gets reflected out of Port 1. S_{22}

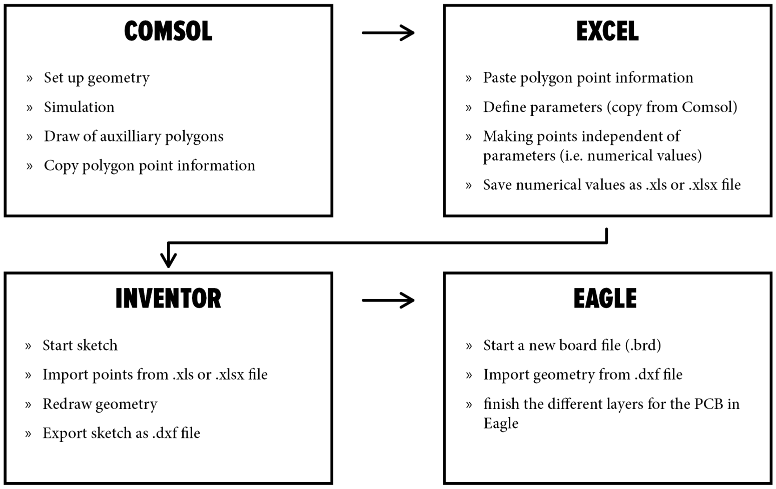

Figure 3.3: A schematic representation of the workflow for getting a geometry from Comsol to Eagle.

does the same for Port 2. We try to minimise these values, because they are a measure of internal reflection in the CPW. The reverse is true for S_{12} and S_{21} (these have for symmetry reasons the same values) which describe what is transmitted through the system, we try to maximise these values. Since these values describe how "smoothly" the microwaves flow through the CPW, we want them to be large - not only because we want to minimze reflections but also because we don't want the CPW to act as an antenna which radiates power to its surroundings. We want to concentrate a large proportion of the energy in the near field.

The second property we are interested in is the radial component of the magnetic field at the position of the caesium BEC. For that reason the radial component of the magnetic field is important see section 2.4. The magnetic field oscillates at this point with the frequency of the incident microwaves. To make good use of the energy put into the system, a minimised nonradial component of the magnetic field is useful.

Therefore the goal of the simulation is to maximise the radial component while at the same time maximising S_{12} (or S_{21}). As it turns out one has to find a useful compromise in the geometry so that both parameters have a decently good value.

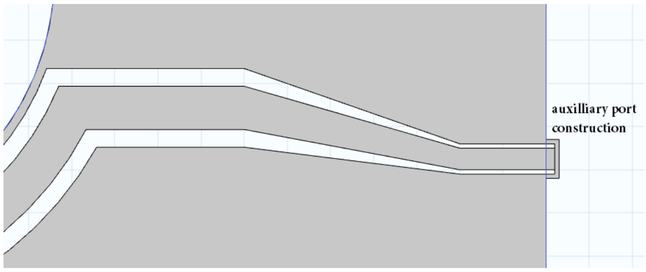

Figure 3.4: The auxilliary port construction used for simulating coplanar waveguides.

3.2.1 Setting up a model

To prepare a model for Comsol that can be studied one has to create a geometry (it is also possible to import a geometry, which is rather straightforward but for our purposes the gemeotry was created from scratch inside Comsol). It is rather straightforward to do this. To have a model that has an easily changeable geometry one has however to take geometric parameters into consideration. In Comsol one has the possibility to define a set of parameters, these can be changed quickly if the geometry is defined in terms of these parameters. One has to be advised to be thorough and careful however, since one single part of the geometry defined in absolute terms can mess up the whole model. This leads to rather tedious terms which for our model require quite a bit of trigonometry.

In general the metallisation of the coplanar waveguide will not be modelled as 3D objects but rather as surfaces that have the boundary condition of perfect electric conductors. The dielectric bulk is assigned to the desired material (in our case Rogers RO4350E). After setting up the base geometry and materials one has to take care to properly define the ports. We followed the Comsol guide for modelling coplanar waveguides [16]. There are three methods to model the ports correctly. In the method chosen, small rectangular faces are added at the areas where the ports are, see figure 3.4. The square bracket shaped border strips have to be assigend as perfect electric conductors as well. The port is set inside the small rectangular face next to the not metallised strips.

After setting up the chip itself one has to take care of its surroundings. That means one has to place the chip inside a sufficently big (in our case ∼10 times the size of the chip itself) sphere of air, which itself has a boundary condition on its outer perimeter so that the radiated electromagnetic fields are not reflected back to the chip. One can either use a *perfectly matched layer* for that or a *periodic boundary condition*. We used a perfectly matched layer which one can imagine as a perfect absorber of electromagnetic radiation.

Before starting a simulation one finally needs to create a mesh. There are basically two options to define a mesh in Comsol, either you define a user-controlled mesh or you give the task of defining your mesh and its resolution in certain areas to Comsol (physics-controlled mesh). We chose the later. It is also recommended that you set a maximum mesh size in free space, which should be smaller than one fifth of the wavelength in free space.

3.2.2 Performing a study

There are a range of different studies available in Comsol. For our case however there basically two different studies we are interested in. On the one hand via a *Frequency Domain Study* one can explore the electric and magnetic fields at a certain frequency. On the other hand an *Adaptive Frequency Sweep* study can be used to examine the S-Parameters.

Frequency Domain Study

A Frequency Domain Study can be used when all input signals are sinusodial. This gives you a complex, static result which can be used to extrapolate a harmonic time dependent solution of the electric and magnetic fields. In simple terms it calculates a snapshot in time which you can modulate with a phase. This phase acts as the time variable. So one can produce a time dependent solution of the harmonic case of the magnetic field at the point of interest (where the caesium atoms will be). One can also produce an animation of the changing fields fields via the Export option.

Compared to the Adaptive Frequency Sweep Study this study is quite quick, because it only has to compute one case with one frequency. For our cases the simulation time was in the order of minutes to tens of minutes.

Adaptive Frequency Sweep Study

Compared to the Frequency Domain the Adaptive Frequency study takes longer (in the order of hours to tens of hours), which is hardly suprising since it simulates not one but a range of frequencies. It however uses a reduced-order model in the frequency domain [17]. For this study one only needs to define a lower and an upper bound to the frequency range one wants to analyse and a step size, which determines how fine the result will be with respect to changes in frequency. We used this study to analyse the S-Parameters.

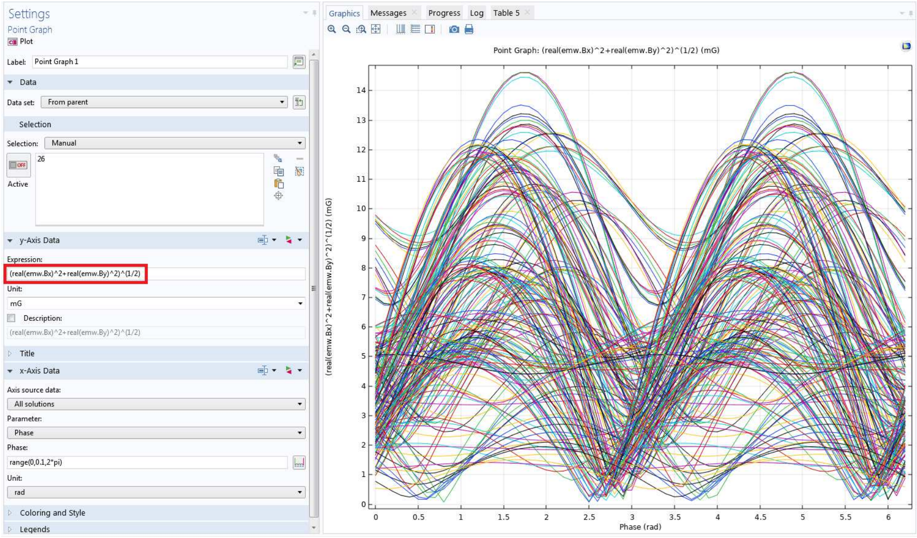

Settings
Point Graph
Plot

Label: Point Graph 1

Data

Data set: From parent

Selection

Selection: Manual

26

Active

y-Axis Data

Expression: (real(emw.Bx)^2+real(emw.By)^2)^(1/2)

Unit: mG

☐ Description: (real(emw.Bx)^2+real(emw.By)^2)^(1/2)

Title

x-Axis Data

Axis source data: All solutions

Parameter: Phase

Phase: range(0,0.1,2*pi)

Unit: rad

Coloring and Style

Legends

Point Graph: (real(emw.Bx)^2+real(emw.By)^2)^(1/2) (mG)

Figure 3.5: Example of a Comsol visualisation in this case the visualisation of the radial component (red box) of a series of different geometries using a parametric sweep.

3.2.3 Visualisation

There are plenty of possibilities to visualise the results of the simulation. One can use 1D, 2D, 3D graphs and other options. A general visualisation of the electric field distribution of a generic straight CPW is given in figure 3.6 (compare also to 2.11). Visualisation of these kind are especially usefull to get a qualitiative picture of what is going on. For a more quantitative approach 1D plots are more usefull. S-Parameters are automatically produced when doing an Adaptive Frequency Sweep Study and can be found under Results → Derived Values → S-Parameter. Custom 1D graphs can also be created. For example what is of interest in our simulation is the magnetic near field configuration at the point where the caesium atoms will be, especially the radial component of the magnetic field relative to symmetry axis and perpendicular to the plane of the CPW.

3.3 Results

In total four different geometries were simulated. Firstly, this was just a straight coplanar waveguide with a constant width, secondly a straight coplanar waveguide which has a tapered profile of the inner metallized strip. The third structure is quite close to the final geometry and differs only in the fact, that it doesn't

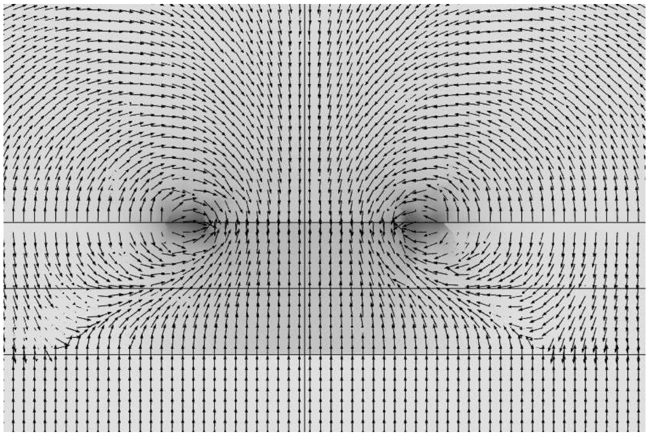

Figure 3.6: Visualisation of the electric field distribution ina vertical cut through the CPW.

contain a milled out hole but instead has a fully metallized inner circle. The final gemeotry has a similiar structure to the outlines of a keyhole. It consists of straight lines which lead from the connector to the main circular element which should produce the appropriate magnetic microwave field. After producing a first version we noticed that the S-parameter for transmission was not constant around 9.19 GHz and also that the S-parameter itself was between -4 dB and -6 dB in the range of 9.15 GHz and 9.25 GHz which is insufficient. We had to redo the simulation with the goal of optimizing the S-parameters. This resulted in an improved version. In the next section the difference in the S-parameters is depicted. The 5 different geometries are shown in figure 3.7.

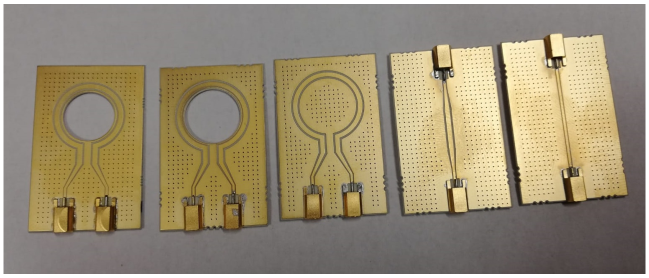

Figure 3.7: The different printed waveguides. From left to right: The new version of the CPW, the old version of the CPW, the CPW structure without hole, the tapered version of the CPW and the straight CPW.

The mini SMP connectors require a 3.2 x 5 mm gap to connect to the semi rigid cable which connects the CPW to the microwave instruments and electronics. These connectors also determine the initial thickness of the inner metallized strip (0.5 mm) which in turn also determines the gap on both sides of the inner strip (see section 2.5.2). To not abruptly change the geometry this thickness is then continiously widened to the best proportions of the inner strip and gap from the simulation, as shown in figure 3.4. The designs were chosen to allow for a systematic study of the individual geometric features and their influence on performance which may result from changes of the characteristic impedance. This can lead to, as discussed in 2.5.2, undesired reflections.

3.3.1 Measurement of S-parameters

Important for the characterisation of the waveguide are, as discussed in 2.5.3, the scattering parameters. These S-parameters are on the one hand calculated in the simulation (in this case the Adaptive Frequency Sweep). On the other hand the S-parameters can be measured with a socalled *vector network analyzer*. We used a keysight E5071C 200 kHz - 20 GHz ENA Series Network Analyzer. With this instrument one can easily measure the S-paramaters. One has, however, to calibrate it with an (ideally) perfect ”through”, i.e. an element which transmits 100 % at all frequencies. We used our simplest, parallel and straight CPW, which which is the cloesest realisiation of a perfect ”through”. One also has to take into account, that the semi-rigid cables with which the waveguide is connected to the vector signal analyzer change their frequency behaviour a little every time they are deformed when connecting a new waveguide. This means that there is no perfect calibration and it is possible, that S-parameters can exceed 0 dB, which is theoretically impossible. This systematic error is on the order of several tenths of dB.

As can be clearly seen in the figures of this section the agreement of measurement and simulation varies significantly between different geometries. In the case of the of the tapered CPW the measurement and the simulation are in good agreement. For the new version of the CPW the simulation shows larger losses than the measurement. This could be because in the simulation radiative losses can become larger due to the fact, that the metallization is represented by an ideal conductor. For the old version of the CPW the simulation shows also a rough agreement with the measurement although the slope with respect to the frequency differs more than with the new version. Finally the CPW without hole shows a completely virtual resonance at 9.02 GHz which is apparently only a numerical artefact.

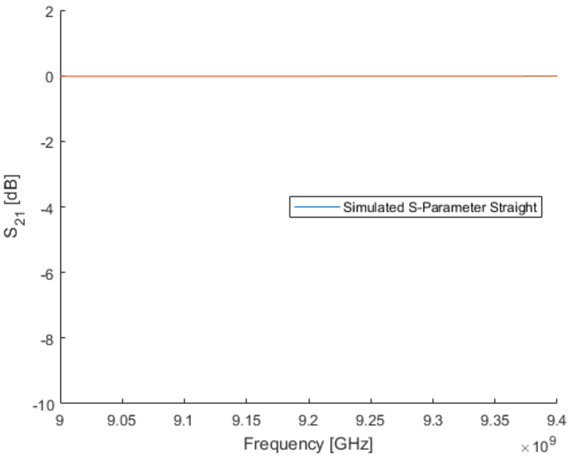

Figure 3.8: For reference the simulated S-parameters of the straight and parallel CPW, it shows a very constant S-parameter of close to 0 dB for transmission.

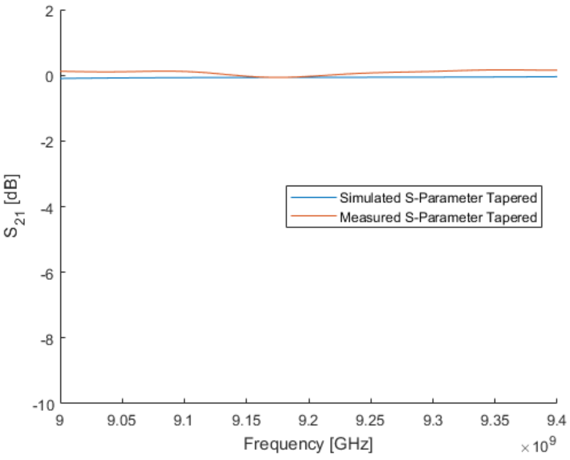

Figure 3.9: S-parameters of the tapered CPW. Measured in red and calculated in blue.

3.3.2 Magnetic Field of the CPWs

The second important property of the waveguides is the magnetic field. The results of the simulation are shown below. The first results are cuts in which the magnetic field strength (color map) and the direction of the field (arrows) are shown. Please note that the length of the arrows is normalized to the same

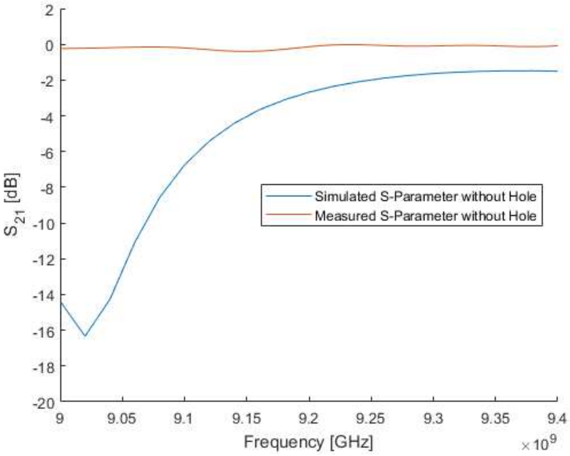

Figure 3.10: S-parameters of the CPW without hole. Measured in red and calculated in blue.

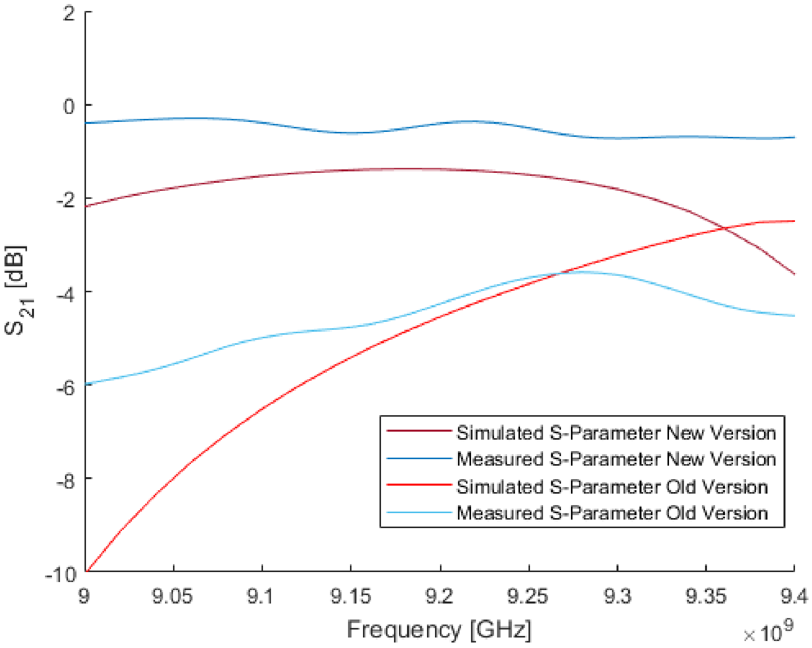

Figure 3.11: S-parameters of the old version and new version of the CPW. Measured in red and calculated in blue.

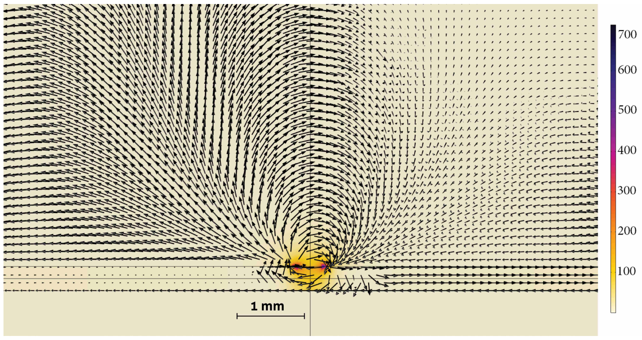

Figure 3.12: Cut through the straight CPW. The unit of the magnetic field is mG. Microwave power is 2 W.

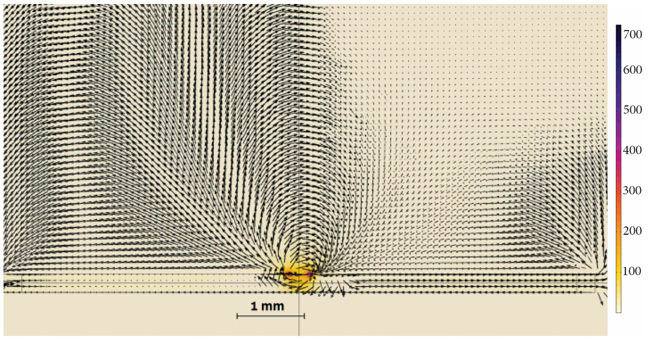

Figure 3.13: Cut through the tapered CPW. The unit of the magnetic field is mG. Microwave power is 2 W. The vectors are normalized.

length because it would span several orders of magnitude, while the magnitude is shown by using a colormap instead. The planes of the cuts are chosen perpendicular to the direction of the microwave. For the straight and the tapered geometry the vertical cut plane is chosen in the propagation centre of the chip. For the CPWs with a circular element it is chosen as perpendicular to the axis of symmetry and going through the center point of the circular part.

It can be clearly seen that the strongest magnetic field is in the gap where the microwave travels. What is more important than these cuts however is the magnetic field strength as a function of distance in the symmetry axis of the circlular element, where the atoms will be positioned. Directly proportional to the magnetic field are the Rabi frequencies between $|4,4\rangle$ and $|3,3\rangle$, they are also given in figures 3.21 and3.22.

One can see from figure 3.20 that at the position of the BEC, approximately 6 mm from the surface of the chip a magnetic field strength of 10 mG can be

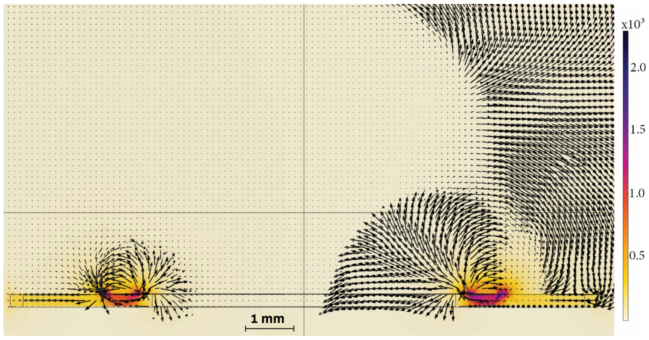

Figure 3.14: Cut through the CPW without hole. The unit of the magnetic field is mG. Microwave power is 2 W. The vectors are normalized.

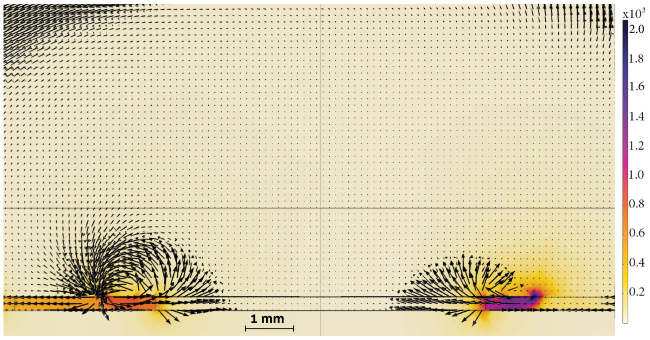

Figure 3.15: Cut through the old version of the CPW. The unit of the magnetic field is mG. Microwave power is 2 W. The vectors are normalized.

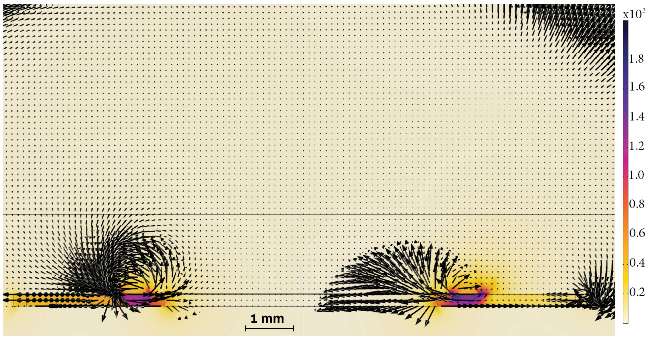

Figure 3.16: Cut through the new version of the CPW. The unit of the magnetic field is mG. Microwave power is 2 W. The vectors are normalized.

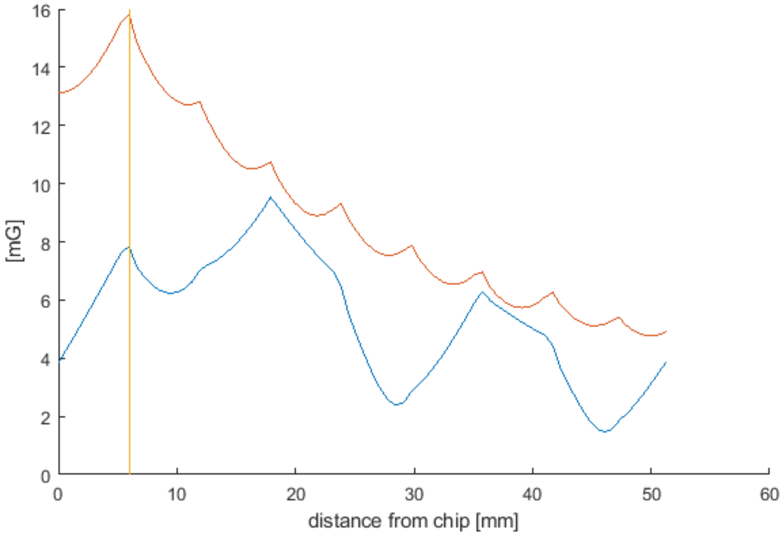

Figure 3.17: The strength of the total magnetic field (red) and the strength of the circular component (blue) as a function of the distance from the surface of the chip with 2 W microwave power for the old version of the CPW. The plot displays one single instant in time and the form of the graph changes over one microwave period. The vertical line denotes the position of the atoms.

expected and also that a large part of the magnetic field at that position is in the radial component. The new geometry also shows a smaller band for the different curves which means that the radial component of the magnetic field produced shows less variation in strength.

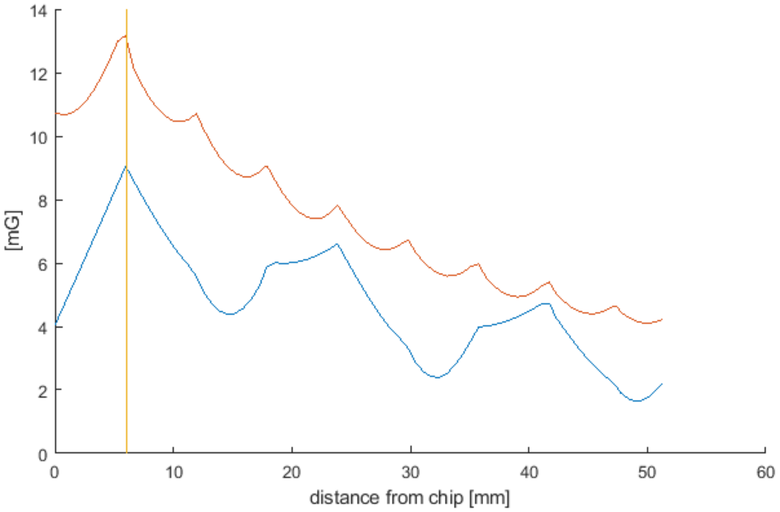

Figure 3.18: The strength of the total magnetic field (red) and the strength of the circular component (blue) as a function of the distance from the surface of the chip with 2 W microwave power for the new version of the CPW. The plot displays one single instant in time and the form of the graph changes over one microwave period. The vertical line denotes the position of the atoms.

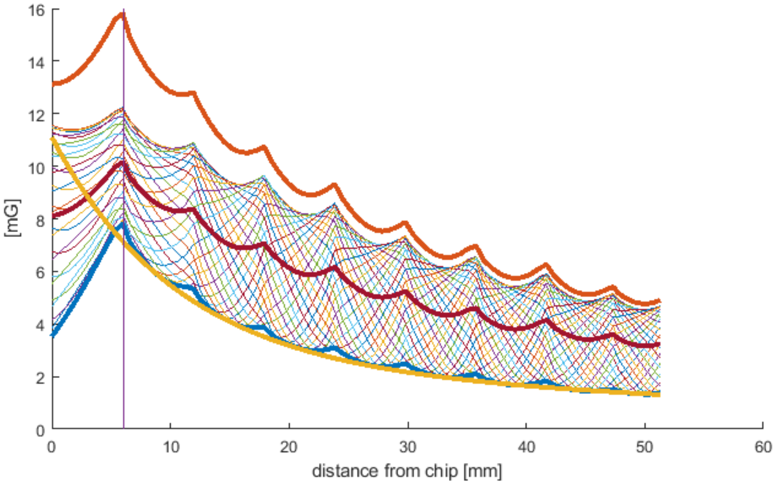

Figure 3.19: The magnetic field of the old version of the CPW for different instances in time for the old version of the CPW. It shows a non-trivial behaviour of the magnetic field. The orange curve shows the total magnetic field, the red curve is the time average of the radial component of the magnetic field, the blue curve shows the minimal strength of the radial component of the magnetic field at any time. As an approximation we used an exponential function which consists of two exponential parts (in this case in units of mG and mm): $B_r(z) = 8.45\ e^{-0.097z} + 2.63\ e^{-0.0144z}$ The vertical line denotes the position of the atoms.

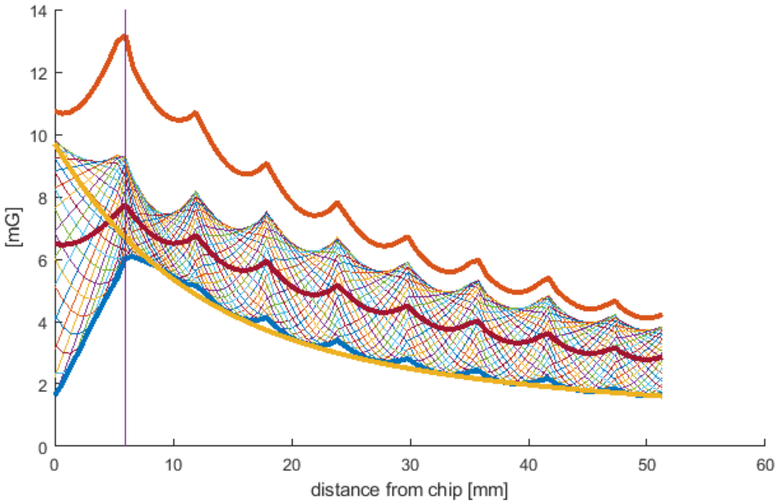

Figure 3.20: The magnetic field of the new version of the CPW for different instances in time for the old version of the CPW. It shows a non-trivial behaviour of the magnetic field. The orange curve shows the total magnetic field, the red curve is the time average of the radial component of the magnetic field, the blue curve shows the minimal strength of the radial component of the magnetic field at any time. As an approximation we used an exponential function which consists of two exponential parts (in this case in units of mG and mm): $B_r(z) = 6.62\, e^{-0.091z} + 3.08\, e^{-0.0134z}$ The vertical line denotes the position of the atoms.

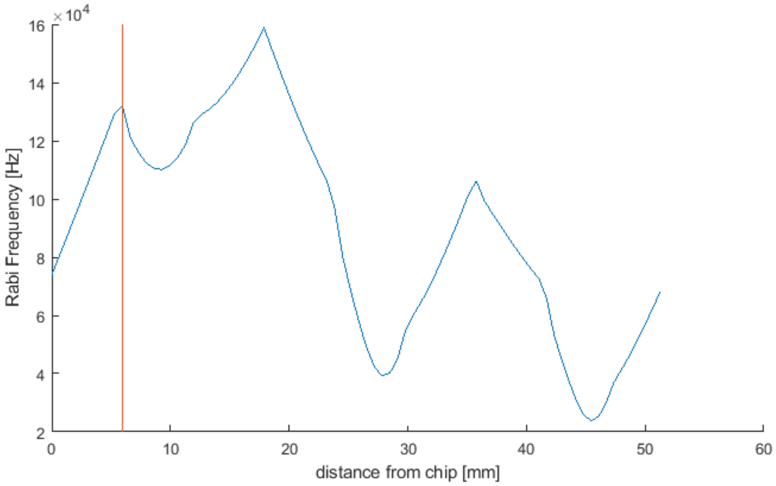

Figure 3.21: The Rabi frequency for the $|4,4\rangle$ to $|3,3\rangle$ transition as a function of the distance from the surface of the chip for the old version of the CPW. The plot displays one single instant in time and the form of the graph changes over one microwave period. The vertical line denotes the position of the atoms.

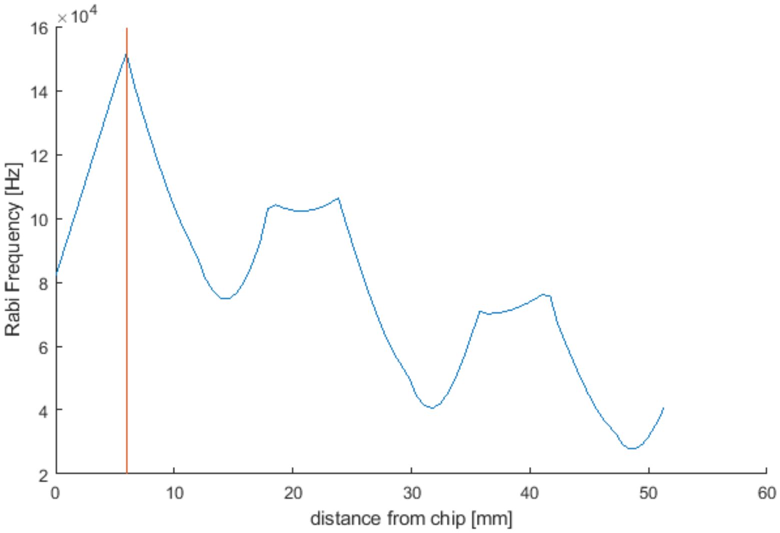

Figure 3.22: The Rabi frequency for the $|4,4\rangle$ to $|3,3\rangle$ transition as a function of the distance from the surface of the chip for the new correct CPW. The plot displays one single instant in time and the form of the graph changes over one microwave period. The vertical line denotes the position of the atoms.

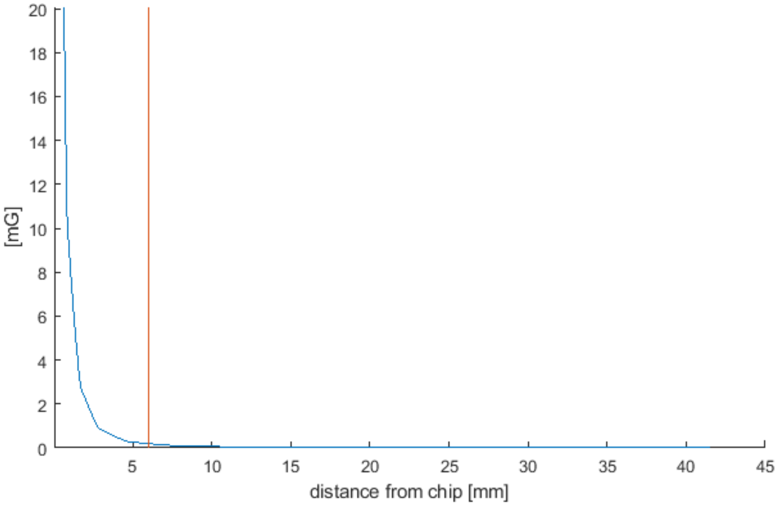

Figure 3.23: The magnetic field of the straight CPW as a function of the distance from the surface of the CPW. As one can see the field decreases very rapidly over the distance. The vertical line denotes the position of the atoms.

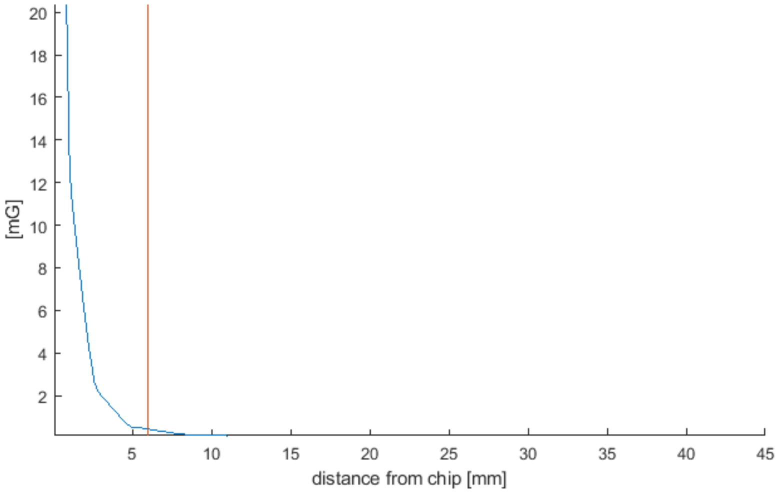

Figure 3.24: The magnetic field of the tapered CPW as a function of the distance from the surface of the CPW. As one can see the field decreases very rapidly over the distance. The vertical line denotes the position of the atoms.

Chapter 4

Measurements of the Coplanar Waveguides

4.1 Microwave Setup

To "power" the coplanar waveguide, i.e. to transmit a microwave at the desired frequency through the waveguide which produces the desired magnetic field at the final point of interest (where the caesium atoms are), a microwave generator and additional electronics for switching and amplification are required.

The microwave setup starts with a microwave generator, in our case a Rohde & Schwarz SMB100A Microwave Signal Generator. With this generator one can produce microwaves at a desired amplitude and frequency. In our case the instrument is remotely controlled via a central instrument control. The signal generator is connected via commercialy produced microwave cable, a CBL-1.5M-SMSM+ Precision Test Cable, to a solid state switch, an AMC SWNLC-DC20-1DT by American Microwave Corporation. This switch allows a control of the microwave signal on a nanosecond scale (25 ns response time and 5 ns rise and fall time), this is also done remotely via a TTL signal. The switch is connected via simple SMA male connectors to the amplifier, a AM25-9-9.4-40-32 by microwave amps. This amplifier has a fixed amplification of 40 dB. The control of the amplitude of the microwave is therefor done via the microwave generator itself. The maximal output of the amplifier is 33 dBM which corresponds to approximately 2 W. It is needed because the microwave generator is only able to produce an output power of 27 dBm. The amplifier - also connected via a SMA male connector - is followed a circulator, a 4015C-30 by Narda-MITEQ. This circluator is needed to ensure that any back reflections don't reach the amplifier, which would likely damage it. The last instrument before the CPW is a

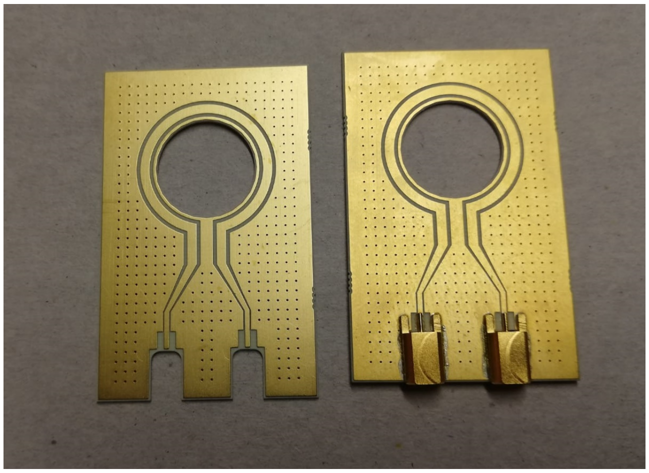

Figure 4.1: The coplanar waveguide structure. On the right without any connectors on the left with mini SMP connectors.

directional coupler (4015C-30 by Narda-MITEQ), which diverts a small amount of the microwave signal (-30 dB) into a microwave power detector, a Rohde & Schwarz NRVS power meter, which is used to monitor the power going into the waveguide. It uses a Rohde & SchwarzNRV-Z54 thermal power sensor with a 25 dB attenuator in front. The waveguide itself (see figure 4.1) is connected via custom made semi-rigid cables to the main output of the directional coupler, these are necessary in this case because it is difficult to reach final position of the CPW. These semi-rigid cables connect via a mini SMP connector to the waveguide. At the output of the waveguide a 50 Ω termination with a heat sink is also connected with custom made semi rigid cable. Figure 4.2 shows the microwave setup in a schematic form.

Taking a look at the losses and amplifications one can easily calculate the total amplification of the different elements of the microwave setup, which results in an amplification of a little bit more than 32 dB between the microwave generator and the CPW.

4.2 Measurement of the Amplifier

The performance of the amplifier was measured on the one hand with respect to the amplification for a varied frequency and on the other hand with respect to the amplification with a varied input power. The results are shown in figure 4.3 and 4.4. In addition to that, different null signals, i.e. where we would expect no power at the power meter. With everything turned off, the signal at the power

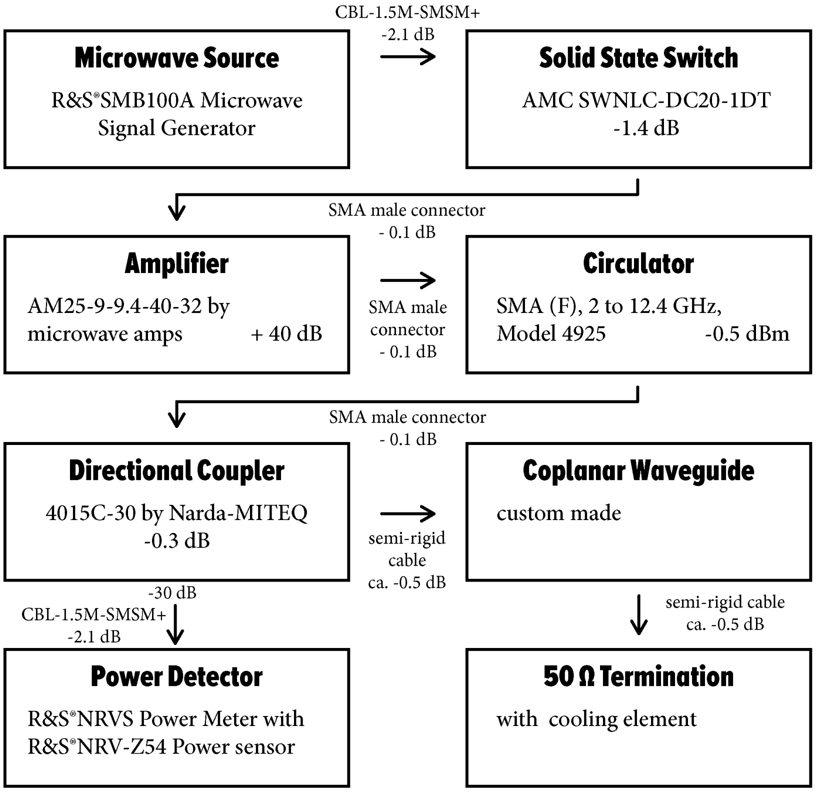

Figure 4.2: The microwave setup in schematic form. The arrows symbolize connections which are specified. The losses and amplifications are given in dB. The losses of the semi rigid cables are only given approximately because they cannot be measured with this setup due to the fact that they only have SMA connectors on one side. The values are estimated from different semi rigid cables with SMA connectors on both ends.

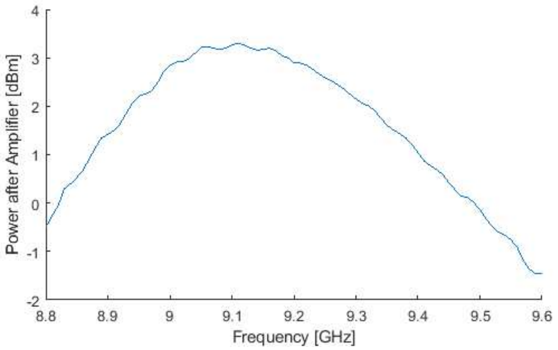

Figure 4.3: The amplification at a constant input power (-30 dBm) for different frequencies.

meter fluctuated between -15 and -13 dBm. The same was true for everything turned off and the switch closed (the default setting is open), it resulted in -15 to -13 dBm at the power meter. When the amplifier was turned on, the signal was between -30 and -20 dBm with sometimes going as low as -40 dBm.

4.3 Power Transmission through CPWs

Similar to the results from section 3.3.1 done with a vector signal analyzer, we could also do our own version of this experiment with our setup. For this the microwave of 9.2 GHz and -10 dBm is generated by the microwave generator, which should result in about 22 dBm at the CPWs. An exact value for the power that goes into the CPW cannot be given since the semi-rigid cables with mini-SMP connectors can only be measured when connected to a CPW. The power of the microwave leaving the CPWs was measured. The comparison of the power of the calculated ingoing signal (22 dBm) and the power of the outgoing signal give a similar result as the measured S-parameters.

new CPW	19.3 dBm
old CPW	12.5 dBm
CPW without hole	20.1 dBm
tapered CPW	20.9 dBm
straight CPW	20.7 dBm

This once again shows the improvement in the S-parameter between the new and the old version of the CPW especially in comparison with the straight and tapered CPW.

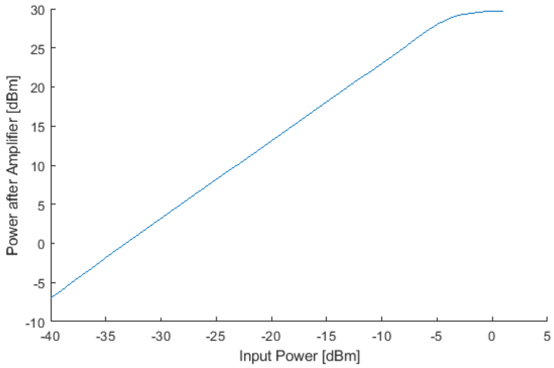

Figure 4.4: The amplification at a constant frequency (9.15 GHz) for different input powers. The output power plateaus at 30 dBm, which corresponds to 33 dBm immediately after the amplifier.

4.4 Plan to measure of the Magnetic Field

There is no ready-made method of measuring the microwave field on an appropriate length scale. About a decade ago a method was developed that uses the fact that the microwaves drive Rabi oscillations. We follow the procedure by Pascal Böhi and Philipp Treutlein [18]. The basic theoretical idea is outlined in 2.2. To summarize it shortly the Rabi frequencies induced by the magnetic component of the microwave field lead to fluctuations in the population of the $|F = 3\rangle$ and the $|F = 4\rangle$ state which can be imaged by a camera-laser set up. In our case, fluorescence imaging is used. The main difference between our setup and the one mentioned in [18] is that due to availability reasons we were unable to use flat caesium cells, but made use of commercially available[1] cylindric cells. That means that the waveguide cannot be placed on top of the thin cell as shown in figure 4.5.

In our setup the CPW is placed at the back of the cell. The laser illuminates the whole cell in the direction of the symmetry axis of the cylinder. With this setup it is not really possible to put the camera behind the CPW structure because it would block most of the light (apart from the hole). It is rather situated ”behind” the principal laser beam (rather perpendicular to it, which is realized via a beam splitter). A schematic illustration of the setup is shown in figure 4.6.

To have more flexibility and options for the measurement the setup includes both laser resonant with the transitions from F=3 and F=4 to the $P_{3/2}$ manifold. These laser are used as ”repump” and ”cooling” lassers in the BEC setup. We

---

[1] The cells were kindly lent ti us by

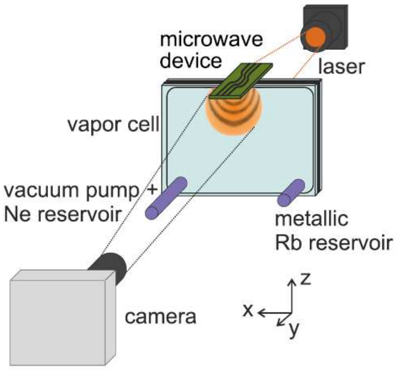

Figure 4.5: The setup from [18] uses a different configuration of laser, cell and CPW.

use two fibre couplers to get the laser beams from our main laser table. Since one of them produces a very small beam width it needs to be broadened via a lens system to illumanite the whole cell. After combining them via a polarized beam splitter the polarization direction is rotated 45° so that in the next polarized beam splitter equal amounts of both laser beams are transmitted. After this beam splitter a quarter-wave plate is used to change the polarization to cirular which is needed to measure the cirular component of the magnetic microwave field. As can be seen in the schematic representation the CPW is situated behind the cell. The laser illuminates the cell and the resulting fluorescence is picked up by a camera situated perpendicular to the main laser axis. While passing back in the direction of the camera the polarization of the light is changed back to linear polarization so it passes through the PBS and is finally picked up by the camera.

At the time of writing the setup for measuring the magnetic field or performing a double resonance microwave spectroscopy [19] is in place, but not yet fully functional. A double resonance spectroscopy would require the transmission through the cell and CPW with a photodiode at the back. The laser is continuously on, while the microwave is varied around the transition from $|3,0\rangle$ to $|4,0\rangle$ which is $\nu_0 \simeq 9.2$ GHz, which is not affected by magnetic fields. In this case the light after the cell and the CPW is picked up by a photo diode and it should change in intensity whenever the microwave signal is close to the resonance of one transition, which would reshuffle the population in the different states (Rabi oscillations). Since we were yet unsuccessful in this respect there will be a short outlook on how to proceed from here.

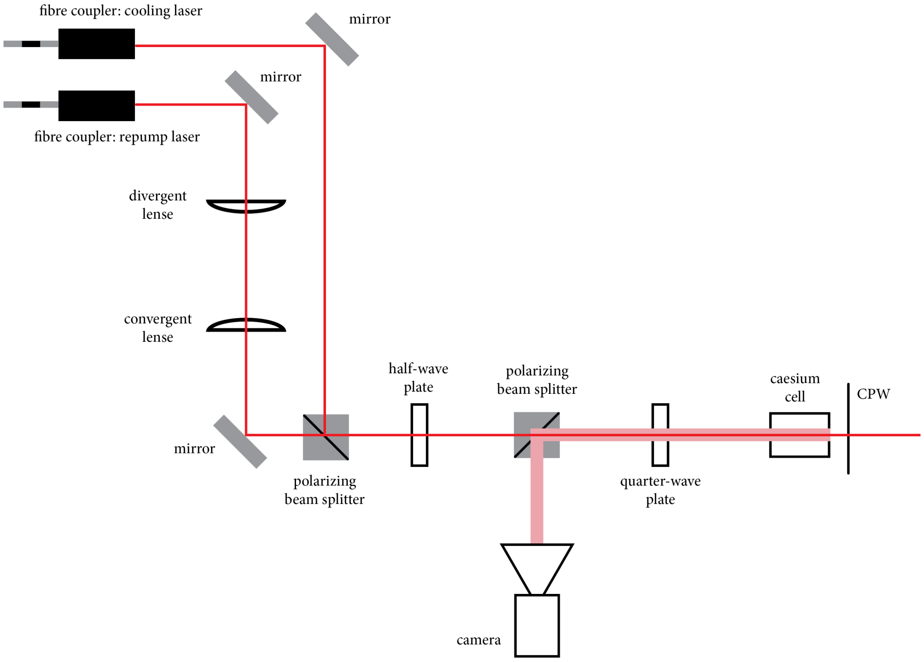

Figure 4.6: A schematic representation of the laser setup with the caesium cell.

Chapter 5

Outlook

From the data we could collect from the simulations and the S-parameter measurements we are confident, that the field behaviour of the CPW should be in general agreement with what was simulated and designed.

As discussed the state of work at this moment is that the field produced by the CPW is not yet picked up by the caesium atoms in any discernible way. This will be worked on further in our group. This means that the first avenue forward will be to try to get the setup to work, then measure Rabi frequencies and relate back to the magnetic field strength produced by the CPW. A faster photo diode for the double resonance spectroscopy or alternatively a more powerful microwave amplifier will assist these efforts.

Should the field measurements show that the CPW is not sufficient, there are several options of how to proceed from here without the current general concept. On the one hand a different geometry of waveguide can be tried. Another option would be a CPW which includes a resonator structure, that could lead to an enhancement in the near field. For example a planar circular spiral inductor (see figure **??**). A patch antenna would be another option. What is of primary importance for the experiment is, that the microwave structure is relatively flat and also allows for an optical access (i.e. transparent or with a hole). For that reason a helical antenna is probably not suitable.

Appendix A

Rabi Frequency calculation

With the Clebsch-Gordan coeefficients the relevant base vectors $|F, m_F\rangle$ for the caesium ground state are given in the $|I, m_I, J, m_J\rangle$ base

$$
\begin{aligned}
|4,-4\rangle &= \left|\frac{7}{2},-\frac{7}{2}\right\rangle \left|\frac{1}{2},-\frac{1}{2}\right\rangle \\
|4,-3\rangle &= \sqrt{\frac{1}{8}}\left|\frac{7}{2},-\frac{7}{2}\right\rangle \left|\frac{1}{2},\frac{1}{2}\right\rangle + \sqrt{\frac{7}{8}}\left|\frac{7}{2},-\frac{5}{2}\right\rangle \left|\frac{1}{2},-\frac{1}{2}\right\rangle \\
|4,-2\rangle &= \sqrt{\frac{1}{4}}\left|\frac{7}{2},-\frac{5}{2}\right\rangle \left|\frac{1}{2},\frac{1}{2}\right\rangle + \sqrt{\frac{3}{4}}\left|\frac{7}{2},-\frac{3}{2}\right\rangle \left|\frac{1}{2},-\frac{1}{2}\right\rangle \\
|4,-1\rangle &= \sqrt{\frac{3}{8}}\left|\frac{7}{2},-\frac{3}{2}\right\rangle \left|\frac{1}{2},\frac{1}{2}\right\rangle + \sqrt{\frac{5}{8}}\left|\frac{7}{2},-\frac{1}{2}\right\rangle \left|\frac{1}{2},-\frac{1}{2}\right\rangle \\
|4,0\rangle &= \sqrt{\frac{1}{2}}\left|\frac{7}{2},-\frac{1}{2}\right\rangle \left|\frac{1}{2},\frac{1}{2}\right\rangle + \sqrt{\frac{1}{2}}\left|\frac{7}{2},\frac{1}{2}\right\rangle \left|\frac{1}{2},-\frac{1}{2}\right\rangle \\
|4,1\rangle &= \sqrt{\frac{5}{8}}\left|\frac{7}{2},\frac{1}{2}\right\rangle \left|\frac{1}{2},\frac{1}{2}\right\rangle + \sqrt{\frac{3}{8}}\left|\frac{7}{2},\frac{3}{2}\right\rangle \left|\frac{1}{2},-\frac{1}{2}\right\rangle \\
|4,2\rangle &= \sqrt{\frac{3}{4}}\left|\frac{7}{2},\frac{3}{2}\right\rangle \left|\frac{1}{2},\frac{1}{2}\right\rangle + \sqrt{\frac{1}{4}}\left|\frac{7}{2},\frac{5}{2}\right\rangle \left|\frac{1}{2},-\frac{1}{2}\right\rangle \\
|4,3\rangle &= \sqrt{\frac{7}{8}}\left|\frac{7}{2},\frac{5}{2}\right\rangle \left|\frac{1}{2},\frac{1}{2}\right\rangle + \sqrt{\frac{1}{8}}\left|\frac{7}{2},\frac{7}{2}\right\rangle \left|\frac{1}{2},-\frac{1}{2}\right\rangle \\
|4,4\rangle &= \left|\frac{7}{2},\frac{7}{2}\right\rangle \left|\frac{1}{2},\frac{1}{2}\right\rangle
\end{aligned}
\tag{A.1}
$$

$$\begin{aligned}
|3,-3\rangle &= -\sqrt{\frac{7}{8}}\left|\frac{7}{2},-\frac{7}{2}\right\rangle\left|\frac{1}{2},\frac{1}{2}\right\rangle+\sqrt{\frac{1}{8}}\left|\frac{7}{2},-\frac{5}{2}\right\rangle\left|\frac{1}{2},-\frac{1}{2}\right\rangle \\
|3,-2\rangle &= -\sqrt{\frac{3}{4}}\left|\frac{7}{2},-\frac{5}{2}\right\rangle\left|\frac{1}{2},\frac{1}{2}\right\rangle+\sqrt{\frac{1}{4}}\left|\frac{7}{2},-\frac{3}{2}\right\rangle\left|\frac{1}{2},-\frac{1}{2}\right\rangle \\
|3,-1\rangle &= -\sqrt{\frac{5}{8}}\left|\frac{7}{2},-\frac{3}{2}\right\rangle\left|\frac{1}{2},\frac{1}{2}\right\rangle+\sqrt{\frac{3}{8}}\left|\frac{7}{2},-\frac{1}{2}\right\rangle\left|\frac{1}{2},-\frac{1}{2}\right\rangle \\
|3,0\rangle &= -\sqrt{\frac{1}{2}}\left|\frac{7}{2},-\frac{1}{2}\right\rangle\left|\frac{1}{2},\frac{1}{2}\right\rangle+\sqrt{\frac{1}{2}}\left|\frac{7}{2},\frac{1}{2}\right\rangle\left|\frac{1}{2},-\frac{1}{2}\right\rangle \qquad \text{(A.2)} \\
|3,1\rangle &= -\sqrt{\frac{3}{8}}\left|\frac{7}{2},\frac{1}{2}\right\rangle\left|\frac{1}{2},\frac{1}{2}\right\rangle+\sqrt{\frac{5}{8}}\left|\frac{7}{2},\frac{3}{2}\right\rangle\left|\frac{1}{2},-\frac{1}{2}\right\rangle \\
|3,2\rangle &= -\sqrt{\frac{1}{4}}\left|\frac{7}{2},\frac{3}{2}\right\rangle\left|\frac{1}{2},\frac{1}{2}\right\rangle+\sqrt{\frac{3}{4}}\left|\frac{7}{2},\frac{5}{2}\right\rangle\left|\frac{1}{2},-\frac{1}{2}\right\rangle \\
|3,3\rangle &= -\sqrt{\frac{1}{8}}\left|\frac{7}{2},\frac{5}{2}\right\rangle\left|\frac{1}{2},\frac{1}{2}\right\rangle+\sqrt{\frac{7}{8}}\left|\frac{7}{2},\frac{7}{2}\right\rangle\left|\frac{1}{2},-\frac{1}{2}\right\rangle \quad .
\end{aligned}$$

With these it is possible to evaluate the operators J_+, J_-, and J_z. The eigenvalues of these three operators are given by

$$\begin{aligned}
J_+\,|J,m_j\rangle &= \sqrt{(J-m_j)(J+m_J+1)}\,|J,m_J+1\rangle \\
J_-\,|J,m_j\rangle &= \sqrt{(J+m_j)(J-m_J+1)}\,|J,m_J-1\rangle \qquad \text{(A.3)} \\
J_z\,|J,m_j\rangle &= m_J\,|J,m_J\rangle \quad .
\end{aligned}$$

With these we can evaluate the matrix elements. To show how this is done we look at an example

$$\begin{aligned}
\langle 4,-3|\,J_-\,|3,-2\rangle = &-\sqrt{\frac{1}{8}}\sqrt{\frac{3}{4}}\left\langle\frac{7}{2},-\frac{7}{2}\right|\left\langle\frac{1}{2},\frac{1}{2}\right|J_-\left|\frac{1}{2},\frac{1}{2}\right\rangle\left|\frac{7}{2},-\frac{5}{2}\right\rangle \\
&-\sqrt{\frac{7}{8}}\sqrt{\frac{3}{4}}\left\langle\frac{7}{2},-\frac{5}{2}\right|\left\langle\frac{1}{2},-\frac{1}{2}\right|J_-\left|\frac{1}{2},\frac{1}{2}\right\rangle\left|\frac{7}{2},-\frac{5}{2}\right\rangle \\
&+\sqrt{\frac{1}{8}}\sqrt{\frac{1}{4}}\left\langle\frac{7}{2},-\frac{7}{2}\right|\left\langle\frac{1}{2},\frac{1}{2}\right|J_-\left|\frac{1}{2},-\frac{1}{2}\right\rangle\left|\frac{7}{2},-\frac{3}{2}\right\rangle \\
&+\sqrt{\frac{7}{8}}\sqrt{\frac{1}{4}}\left\langle\frac{7}{2},-\frac{5}{2}\right|\left\langle\frac{1}{2},-\frac{1}{2}\right|J_-\left|\frac{1}{2},-\frac{1}{2}\right\rangle\left|\frac{7}{2},-\frac{3}{2}\right\rangle \quad . \\
&\qquad \text{(A.4)}
\end{aligned}$$

One can easily see that the first, third and fourth term equal zero because the I's and m_I's (the outer bra-ket vectors) don't match and are not changed by J_- which acts only on $|J, m_J\rangle$. Therefore

$$\langle 4,-3|\, J_-\, |3,-2\rangle = -\sqrt{\frac{7}{8}}\sqrt{\frac{3}{4}} \left\langle \frac{7}{2},-\frac{5}{2}\right| \left\langle \frac{1}{2},-\frac{1}{2}\right| J_- \left|\frac{1}{2},\frac{1}{2}\right\rangle \left|\frac{7}{2},-\frac{5}{2}\right\rangle . \tag{A.5}$$

This term can be evaluated with A.3

$$\begin{aligned}\langle 4,-3|\, J_-\, |3,-2\rangle &= -\sqrt{\frac{7}{8}}\sqrt{\frac{3}{4}} \left\langle \frac{7}{2},-\frac{5}{2}\right| \mathbb{1} \left|\frac{7}{2},-\frac{5}{2}\right\rangle \left\langle \frac{1}{2},-\frac{1}{2}\right| J_- \left|\frac{1}{2},\frac{1}{2}\right\rangle \\ &= -\sqrt{\frac{7}{8}}\sqrt{\frac{3}{4}} \left\langle \frac{1}{2},-\frac{1}{2}\right| J_- \left|\frac{1}{2},\frac{1}{2}\right\rangle \\ &= -\sqrt{\frac{7}{8}}\sqrt{\frac{3}{4}} \left\langle \frac{1}{2},-\frac{1}{2}\right| \sqrt{(\frac{1}{2}+\frac{1}{2})(\frac{1}{2}-\frac{1}{2}+1)} \left|\frac{1}{2},-\frac{1}{2}\right\rangle \\ &= -\sqrt{\frac{7}{8}}\sqrt{\frac{3}{4}} = -\sqrt{\frac{21}{32}} \qquad .\end{aligned} \tag{A.6}$$

The nonzero elements are

$$\begin{aligned}\langle 4,-4|\, J_-\, |3,-3\rangle &= -\sqrt{\frac{7}{8}} \\ \langle 4,-3|\, J_-\, |3,-2\rangle &= -\sqrt{\frac{3}{4}}\sqrt{\frac{7}{8}} = -\sqrt{\frac{21}{32}} \\ \langle 4,-2|\, J_-\, |3,-1\rangle &= -\sqrt{\frac{5}{8}}\sqrt{\frac{3}{4}} = -\sqrt{\frac{15}{32}} \\ \langle 4,-1|\, J_-\, |3,0\rangle &= -\sqrt{\frac{1}{2}}\sqrt{\frac{5}{8}} = -\sqrt{\frac{5}{16}} \\ \langle 4,0|\, J_-\, |3,1\rangle &= -\sqrt{\frac{3}{8}}\sqrt{\frac{1}{2}} = -\sqrt{\frac{3}{16}} \\ \langle 4,1|\, J_-\, |3,2\rangle &= -\sqrt{\frac{1}{4}}\sqrt{\frac{3}{8}} = -\sqrt{\frac{3}{32}} \\ \langle 4,2|\, J_-\, |3,3\rangle &= -\sqrt{\frac{1}{8}}\sqrt{\frac{1}{4}} = -\sqrt{\frac{1}{32}} \qquad .\end{aligned} \tag{A.7}$$

$$
\begin{aligned}
\langle 4,-3|\, J_z \,|3,-3\rangle &= -\frac{1}{2}\sqrt{\frac{7}{8}}\sqrt{\frac{1}{8}} - \frac{1}{2}\sqrt{\frac{1}{8}}\sqrt{\frac{7}{8}} = -\sqrt{\frac{7}{64}} \\
\langle 4,-2|\, J_z \,|3,-2\rangle &= -\frac{1}{2}\sqrt{\frac{3}{4}}\sqrt{\frac{1}{4}} - \frac{1}{2}\sqrt{\frac{1}{4}}\sqrt{\frac{3}{4}} = -\sqrt{\frac{3}{16}} \\
\langle 4,-1|\, J_z \,|3,-1\rangle &= -\frac{1}{2}\sqrt{\frac{5}{8}}\sqrt{\frac{3}{8}} - \frac{1}{2}\sqrt{\frac{3}{8}}\sqrt{\frac{5}{8}} = -\sqrt{\frac{15}{64}} \\
\langle 4,0|\, J_z \,|3,0\rangle &= -\frac{1}{2}\sqrt{\frac{1}{2}}\sqrt{\frac{1}{2}} - \frac{1}{2}\sqrt{\frac{1}{2}}\sqrt{\frac{1}{2}} = -\frac{1}{2} \\
\langle 4,1|\, J_z \,|3,1\rangle &= -\frac{1}{2}\sqrt{\frac{3}{8}}\sqrt{\frac{5}{8}} - \frac{1}{2}\sqrt{\frac{5}{8}}\sqrt{\frac{3}{8}} = -\sqrt{\frac{15}{64}} \\
\langle 4,2|\, J_z \,|3,2\rangle &= -\frac{1}{2}\sqrt{\frac{1}{4}}\sqrt{\frac{3}{4}} - \frac{1}{2}\sqrt{\frac{3}{4}}\sqrt{\frac{1}{4}} = -\sqrt{\frac{3}{16}} \\
\langle 4,3|\, J_z \,|3,3\rangle &= -\frac{1}{2}\sqrt{\frac{1}{8}}\sqrt{\frac{7}{8}} - \frac{1}{2}\sqrt{\frac{7}{8}}\sqrt{\frac{1}{8}} = -\sqrt{\frac{7}{64}}
\end{aligned}
\tag{A.8}
$$

$$
\begin{aligned}
\langle 4,-2|\, J_+ \,|3,-3\rangle &= \sqrt{\frac{1}{8}}\sqrt{\frac{1}{4}} = \sqrt{\frac{1}{32}} \\
\langle 4,-1|\, J_+ \,|3,-2\rangle &= \sqrt{\frac{1}{4}}\sqrt{\frac{3}{8}} = \sqrt{\frac{3}{32}} \\
\langle 4,0|\, J_+ \,|3,-1\rangle &= \sqrt{\frac{3}{8}}\sqrt{\frac{1}{2}} = \sqrt{\frac{3}{16}} \\
\langle 4,1|\, J_+ \,|3,0\rangle &= \sqrt{\frac{1}{2}}\sqrt{\frac{5}{8}} = \sqrt{\frac{5}{16}} \\
\langle 4,2|\, J_+ \,|3,1\rangle &= \sqrt{\frac{5}{8}}\sqrt{\frac{3}{4}} = \sqrt{\frac{15}{32}} \\
\langle 4,3|\, J_+ \,|3,2\rangle &= \sqrt{\frac{3}{4}}\sqrt{\frac{7}{8}} = \sqrt{\frac{21}{32}} \\
\langle 4,4|\, J_+ \,|3,3\rangle &= \sqrt{\frac{7}{8}} \qquad .
\end{aligned}
\tag{A.9}
$$

Appendix B

CPW manufacturing specifications

We assigned Multi Circuit Boards to manufacture our CPWs. They have a variety of specifications for design [21]. However we will compactly outline the most important issues, that should be followed. One has to define different layers of the PCB. Layer 1 defines the metallization of the top, this is also where the defining features of the CPW are implemented. Layer 16 defines the metallization of the bottom, vias are defined in layer 16. We used vias with a width of 0.2 mm. In layer 20 the dimension of the PCB is defined (here the gaps for the mini SMP connectors are also defined), there should be a 0.2 mm gap to the metallization layer. In layer 46 one can define milling, which is used to create the hole in the CPW. For the metallized layer a line width of 0.1 mm should be used.

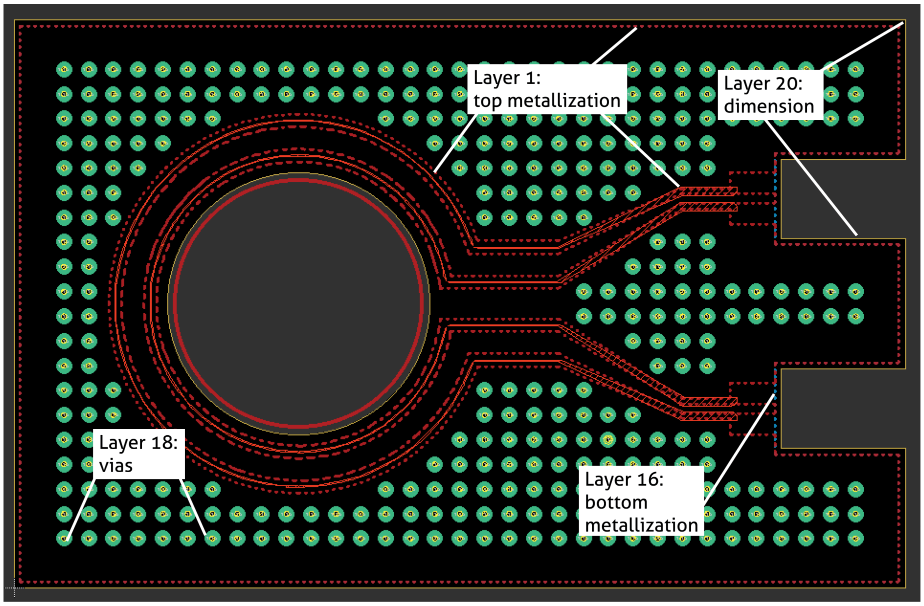

Figure B.1: The different layers in EAGLE. The milling layer 46 cannot be shown in this image, but is approximately where the inner red circle is.

Bibliography

[1] Maximilian Lerchbaumer. Optical dipole trap for a caesium Bose-Einstein condensate, 2018.

[2] Tino Weber. *Bose-Einstein condensation of optically trapped cesium*. na, 2003.

[3] Wolfgang Demtröder. *Experimentalphysik 3: Atome, Moleküle und Festkörper*. Springer-Verlag, 2016.

[4] Daniel A Steck. Cesium d line data, 2003.

[5] Pascal Alexander Böhi. *Coherent manipulation of ultracold atoms with microwave near-fields*. PhD thesis, lmu, 2010.

[6] Christopher J Foot et al. *Atomic physics*, volume 7. Oxford University Press, 2005.

[7] David Papoular. *Manipulation des interactions dans les gaz quantiques: approche théorique*. PhD thesis, Paris 11, 2011.

[8] Claude Cohen-Tannoudji, Frank Laloe, and Bernard Diu. Quantum mechanics. 2019.

[9] DJ Papoular, GV Shlyapnikov, and J Dalibard. Microwave-induced fano-feshbach resonances. *Physical Review A*, 81(4):041603, 2010.

[10] Cheng P Wen. Coplanar waveguide: A surface strip transmission line suitable for nonreciprocal gyromagnetic device applications. *IEEE Transactions on Microwave Theory and Techniques*, 17(12):1087–1090, 1969.

[11] Rainee Simons and RAINEE N Simons. *Coplanar waveguide circuits, components, and systems*. Wiley Online Library, 2001.

[12] David M Pozar. *Microwave engineering*. John Wiley & Sons, 2009.

[13] Spartak Gevorgian, LJ Peter Linner, and Erik L Kollberg. Cad models for shielded multilayered cpw. *IEEE transactions on microwave theory and techniques*, 43(4):772–779, 1995.

[14] Coplanar waveguide calculator. https://www.microwaves101.com/calculators/864-coplanar-waveguide-calculator. accessed 9.8.2019.

[15] Coplanar waveguide analysis/synthesis calculator. http://wcalc.sourceforge.net/cgi-bin/coplanar.cgi. accessed 9.8.2019.

[16] Modeling of coplanar waveguides. https://www.comsol.com/blogs/modeling-coplanar-waveguides/. accessed 6.2.2020.

[17] Comsol rf module. https://www.comsol.com/release/5.3a/rf-module. accessed 12.8.2019.

[18] Pascal Böhi and Philipp Treutlein. Simple microwave field imaging technique using hot atomic vapor cells. *Applied physics letters*, 101(18):181107, 2012.

[19] M Gharavipour, C Affolderbach, S Kang, and G Mileti. Double-resonance spectroscopy in rubidium vapour-cells for high performance and miniature atomic clocks. In *Journal of Physics: Conference Series*, volume 793, page 012007. IOP Publishing, 2017.

[20] Brian C Wadell. *Transmission line design handbook*. Artech House, 1991.

[21] Design aid. https://www.multi-circuit-boards.eu/en/pcb-design-aid/introduction.html. accessed 6.2.2020.